Sl. No.	**IIT Ropar** **List of Recent Publications with Abstract** **Coverage: August, 2024**
A	**Book Chapter(s)**
1.	An effective CNN-based approach for synthetic face image detection in pre-social and post-social media context **P Dey, AS Jadhav, K Rana** - Computer Vision and Image Processing: Books Chapter, 2024 Abstract: The proliferation of image manipulation techniques, including DeepFake technology, has posed significant threats to the authenticity and credibility of images. Accurately classifying real and fake images has become crucial in fields such as forensics, security, and media authentication. However, detecting fake images during downloading and uploading from social networks is even more challenging. In this paper, we present an approach based on the EfficientNet model to learn discriminative features for classifying real and synthetic face images shared on social networks. We conducted extensive experiments using the TrueFace dataset, which comprises real and synthetic facial images shared on three major social media platforms. We employed the EfficientNet-B2 model trained on a combination of pre-social and post-social images from the TrueFace dataset. The presented approach outperforms all other methods, achieving accuracies of 99.98%, 100%, and 100% for images shared on Facebook, Telegram, and Twitter. This approach demonstrates exceptional performance when evaluated on a distinct dataset of images shared on social media platforms, separate from the images used for training.
2.	Application of microwave heating in polymer composites manufacturing **P Bhowmik** - Composite Materials Processing Using Microwave Heating Technology**: Book Chapter, 2024** **Abstract:** Polymer composites have transformed industries with their exceptional properties, but conventional manufacturing processes face challenges such as long processing times, high energy consumption, and environmental concerns. Microwave heating has emerged as a promising technology for polymer composites manufacturing. It utilizes electromagnetic waves to generate heat within materials, offering advantages such as rapid and selective heating, high energy efficiency, and improved control. The benefits of microwave heating include reduced processing time, expedited curing and consolidation processes, and enhanced mechanical properties through improved dispersion and bonding. Challenges remain in optimizing processing parameters, designing microwave-absorbing materials, and ensuring safety. Microwave heating offers rapid and selective heating, enhanced composite properties, and reduced processing time. Ongoing research aims to unlock its full potential in advanced polymer composites production. Microwave heating has the potential to shape the future of polymer composites in various industries by improving efficiency and performance.
3.	Determining critical wall angle in micro-incremental sheet forming of SS316L foils for formability **M Pal, V Pandya, CK Nirala, A Agrawal** - Numerical Methods in Industrial Forming Processes (Numiform- 2023): Book Chapter, 2024 **Abstract:** Micro-incremental sheet forming (μISF) has advantages over existing micro-forming processes (due to its die-less nature of material deformation) and vast applications in sophisticated industries. In μISF, a flexible ultra-thin sheet (foil) is plastically deformed into a complex 3D geometrical shaped component. It is precisely governed by the user-defined toolpath of the forming tool on the surface of the foil. This study investigated the deformation behavior of 100-μm-thick SS316L foils; the foils were deformed into small conical shapes with a tool-tip

with a radius of 500 μm. The μISF process set-up consisted of a rigid fixture to avoid any unwanted distortions during the forming. To test the formability of the foils at different working parameters, experimental and numerical examinations were conducted by varying the wall angle (α = 45°, 60°, 75°) of the forming with three different step depths (z = 10, 20, and 30 μm). A finite element analysis of the process was carried out using ABAQUS® software; the results revealed that the forming angle in μISF had a direct relationship with the formability of the material. Higher values of the step depth assisted in increasing the formability of the SS316L foils. To examine the critical wall angle (α_{cr}) and critical foil thickness (t_{cr}) at the fracture location, a higher range of α (70°–74°) was selected in order to establish a correlation with the depth of the forming.

4.	**Exploring fundamentals: Theory of machines and mechanism inversions**

Exploring fundamentals: Theory of machines and mechanism inversions
S Kumar, P Sarkar - Futuristic Trends in Mechanical Engineering Volume 3 Book 3: Book Chapter, 2024

Abstract: The kingdom of Mechanical Engineering is closely knotted with the principles governing motion, transformation, and the complex interactions within machines and mechanisms. This chapter explores the foundational aspects of "Theory of Machines and Mechanism Inversions". Theory of Machines forms the foundation of Mechanical Engineering, encompassing dynamics, kinematics, and mechanism classifications. This chapter explores into its core, highlighting mobility, degrees of freedom, and linkage between mechanisms and functions. Mechanism Inversions, a captivating concept, involves reconfiguring components to achieve diverse functionalities. Here, we are examining kinematic inversions in planar and spatial mechanisms, showcasing their adaptability in domains like robotics and automotive engineering. By altering arrangements, engineers can innovate and tailor designs to specific needs. In conclusion, this research offers insights into the fundamental "Theory of Machines and Mechanism Inversions". By elucidating these concepts, it paves the way for innovative mechanical engineering solutions, underpinning how engineers analyze, optimize, and conceptualize mechanical systems.

Frugality and sustainability: Essential concepts for sustainable manufacturing
R Kour - Sustainable Manufacturing: Book Chapter, 2024

Abstract: The concepts of frugality and sustainability have been around for centuries, but their relevance has only increased over time. It is important to revive these concepts due to their historical significance and the pressing need to address environmental and social challenges. Frugality, with its focus on simplicity, waste reduction and resourcefulness, has a positive relationship with sustainability. The principles of frugality can broaden the scope of sustainable innovation, making it accessible to all, particularly those in developing countries. The chapter highlights many successful examples of frugal innovation from diverse cultures to demonstrate its practicality in fulfilling sustainable goals. It will also explore how frugality and sustainability can contribute to making sustainable manufacturing more transparent, engaged, cost-effective, and environmentally friendly. By integrating these principles into manufacturing processes, we can create products that meet the needs of consumers while minimizing negative impacts on the environment.

Lab-on-a-chip: A novel platform for disease diagnosis
R Rani, ME Jinugu, **P Gangwar** - Lab-on-a-chip Devices for Advanced Biomedicines: Laboratory Scale Engineering to Clinical Ecosystem: Book Chapter, 2024

Abstract: Medical research has placed a higher value over the last several decades on the detection and investigation of risk associated with disease and biomarkers, which has contributed to more timely and precise tools for diagnosis before the condition worsens. Therefore, a significant amount of time has been utilized in designing and creating detecting technology that will be utilized at the point-of-care to find particular biomarkers without wasting many samples

	such as microfluidic devices. This technology allows for efficient, rapid and high throughput sample analysis, while having multiplexing capability. Commercial lateral flow kits are one of the prominent examples of these microfluidic devices. This chapter discusses in depth the various aspects of microfluidic devices. The chapter covers various microfluidic devices such as paper and chip-based devices and use of these for the diagnostic platform development. This includes the development of electrochemical and optical sensors in a microfluidic setting. The chapter also discusses the future scope for microfluidic device development, especially in wearable fashion.
7.	Sustainable hybrid-reinforced metal matrix composites: A review of production and characterization P. P. Ikubanni, A. A. Adeleke, M. Oki, **H Singh** - Sustainable Manufacturing: Book Chapter, 2024 **Abstract:** The development of advanced engineering materials for various utilizations in different industries is the current thrust of research for materials scientists and engineers. These developed advanced materials have been compared with relevant specifications to ascertain their most preferred areas of utilization. Among the most researched metal matrix for advanced materials development is aluminum, which is always impregnated with various reinforcements (monolithic or hybrid) to produce metal matrix composites (MMCs). These products are lightweight, cost-effective, stronger, and flexible in areas of application. The sustainability of the improvement of advanced materials is a subject of concern; hence, this study compiled some previous studies in this regard. Aluminum MMCs studies are reviewed to indicate various methods of production, hybrid reinforcements in a metal matrix, physical, mechanical, and tribological properties, areas of utilization, and some corrosion studies on MMCs. The study also considered specifically palm kernel shell (PKS) and PKS ash (PKSA) as useful reinforcements in MMCs development. Future areas for aluminum MMCs development and utilization are highlighted.
8.	Sustainable innovations in nanofiber fabrication **S Bhattacharjee**, H Singh, AA Adeleke, PP Ikubanni - Sustainable Manufacturing: Book Chapter, 2024 **Abstract:** Nanotechnology is a vast field that deals with the designs, followed by production, and also the application of various structures, devices, and systems in the nanoscale – i.e., dimensions in the range of 1–100 nm. One of the best aspects of nanotechnology is that materials can be tailored as per the demand, which is termed a bottom-up approach. This key feature allows us to explore more in the areas of 3D printing like bioprinting. To assist in the fabrication of 3D components of any engineering structure or biomedical application, nanofibers play an important role. The nanofiber properties depend largely on the fabrication procedure followed and their process parameters like temperature, catalyst, etc. Hence, techniques used in nanofiber fabrication require optimization based on their applications. In the field of bioengineering and biomedical devices, coatings, in vitro 3D models, filtration membranes, tissues, and scaffolds can be fabricated. Concerning that, various new trends in nanofiber fabrication, like freeze-drying, template synthesis, thermal-induced phase separation, etc., have been discussed in this chapter. Furthermore, these nanofibers can be used for Nobel applications such as the fabrication of bandages specially equipped for rapid wound healing. More such examples have been discussed in detail, along with the difficulties faced during the implementation of these fabrication techniques have been mentioned briefly.
9.	Sustainable production of sponge iron through direct reduction process: Waste recovery from mill scale AA Adeleke, PP Ikubanni…**H Singh…** - Sustainable Manufacturing: Book Chapter, 2024 **Abstract:** This study explored production routes of sponge iron from mill scale via a direct reduction process. Mill scale is termed as industrial waste from an ironmaking process, which is

	often discarded. However, it has been found to be a rich iron-bearing material that can be reprocessed by reduction using lean-grade coal and upgraded biomass as carbonaceous materials. Various direct reduction processes were highlighted, while different iron-bearing materials were exegetically discussed. Different classes and categories of wastes from blast furnaces that are raw materials for sponge iron production were reviewed. The use of torrefied biomass and lean-grade coal as co-reductant in reducing mill scale and other iron-bearing materials were recommended as future paths in the iron and steel industry.
10.	The evolution of influencer marketing A Ahmed, T Rathore - Advances in Data Analytics for Influencer Marketing: An Interdisciplinary Approach: Book Chapter, 2024 **Abstract:** Influencer marketing (IM) is more than just a buzzword. In recent years, IM has gained widespread attention, but its roots actually extend further back than many realize. With the rise of the internet and the explosion of social media, IM has evolved into a new and influential form of marketing communication utilized by businesses of all types. This chapter delves into the historical development of IM, tracing its origins and evolution. We also explore the shift from traditional celebrity endorsements to influencer marketing, providing a comparison of these two endorsement forms. Additionally, we examine the maturation of the IM industry, addressing the challenges and opportunities it presents for marketers. The chapter concludes by addressing current issues in the IM industry, offering a comprehensive and informative look at the phenomena and concepts surrounding IM. Throughout, we strive to provide a thorough explanation of these phenomena, drawing from academic literature and theory to enhance understanding.
B	**Conference Proceeding(s)**
11.	A 0.006 mm^2 low input capacitance low power fully differential neural amplifier S Sharma, Shivdeep, N Sharma, DM Das - 31st International Conference on Mixed Design of Integrated Circuits and System (MIXDES), 2024 **Abstract**: Neural amplifiers are desired to have ultra low power, low noise, low area, high input impedance, band pass response and high CMRR. Capacitively coupled instrumentation amplifier (CCIA) is a widely used topology as it features high power efficiency and moderate area, CMRR and input impedance. The main idea of area minimization relies on the minimum value implementation of the feedback capacitor of the CCIA and optimum mid band gain. We have proposed a feedback network which gives better mismatch for a given equivalent feedback capacitor which allows us to minimize the feedback capacitance without degrading the CMRR and gain mismatch. The amplifier implemented in 180 nm CMOS technology has among the lowest reported area of 0.006 mm^{2} and has an input capacitance of 1 pF. The amplifier consumes 1.08 μW of power and has an NEF of 5.2 with input referred noise of 12.4 μV in 1 - 5 KHz bandwidth. The post layout simulation results of the amplifier are presented.
12.	A 15.4 ppm/°C improved current mode bandgap with 0.9 V supply in 28 nm CMOS MK Singh, H Mehra, T Kaur, R Nagulapalli, DM Das, M Sakare - 2024 International Conference on Integrated Circuits Communication, and Computing Systems (ICIC3S), 2024 **Abstract:** Conventional current-mode bandgap reference (BGR) (Banba) architecture has several issues, like multiple oper-ating points and the need for PTAT current. This paper presents a modified low-voltage Banba architecture using the resistors technique to produce the sub-1 V output. In the Banba BGR, the opamp's offset impacts the output temperature coefficient (TC) due to the low PTAT gain. A high-gain self-bias opamp has been proposed in this research to reduce its effects on BGR TC. The maximum operating voltage of the BGR is analyzed and strongly depends on the bias current; hence, a very low current is used. Post-layout simulations of

the proposed BGR are carried out using 28 nm CMOS technology. A target output voltage is 250 m V, and 15.4 ppml° C is the TC. The proposed BGR output has a standard deviation of 1.3mV based on 200 Monte Carlo simulations. The proposed BGR, with decoupling capacitors included, takes up 3690 μm ^{2} of silicon area and uses 11.7 μW of power from a nominal supply of 0.9V. Compared to conventional and other state-of-the-art BGRs, the proposed BGR has a superior Power Supply Rejection Ratio (PSRR) (around the loop bandwidth) by an increase of 12 dB.

13.	A 66 μw Asynchronous time-domain bulk-tuned offset cancellation circuit for high-precision dynamic comparator

A 66 μw Asynchronous time-domain bulk-tuned offset cancellation circuit for high-precision dynamic comparator

N Sharma, S Sharma, DM Das - 31st International Conference on Mixed Design of Integrated Circuits and System (MIXDES), 2024

Abstract: This paper proposes a novel asynchronous high-precision, low-power, time-domain bulk-tuned offset cancellation technique for high-speed dynamic comparator. The proposed offset cancellation technique minimizes the offset by using bulk-tuning in conjunction with offset sampling in the time domain. The proposed phase detector eliminates the dead zone and is symmetric to both outputs. An energy and area-efficient charge pump with offset polarity-based selectivity is also introduced. The proposed offset cancellation scheme is implemented in 65-nm CMOS technology with a 1.2 V supply, and analytical modeling of the time difference of comparator outputs and offset is also presented. The proposed design has a power consumption of 65.8 μW and maintains a calibration speed of 1 GHz with the comparator operating at 2 GHz frequency. The standard deviation of the offset is decreased to 33.3 μV from 2.183 mV, qualifying it for high-speed, high-precision applications.

A 66dBΩ 5 GHz and 44.88√ Hz/(pA· pW) inductorless TIA in 65 nm CMOS

AY NJ, Shivdeep, S Sharma, H Shrimali, DM Das - 31st International Conference on Mixed Design of Integrated Circuits and System (MIXDES), 2024

Abstract: High-speed optical applications demand broadband transimpedance amplifiers (TIA) for efficient current-to-voltage conversion of photodiode signals. The inherent junction capacitance of photodiodes limits TIA bandwidth. This work proposes an inductorless design strategy for broadband CMOS TIAs. To mitigate the deteriorating effect of photodiode capacitance, a cross-coupled impedance negator integrated with an auxiliary amplifier to form the modified regulated cascode structure (RGC) is utilized at the input stage and, a capacitive degeneration stage is incorporated to improve the bandwidth. The TIA is designed for a high transimpedance gain of 66 dBΩ and is implemented in standard 65nm CMOS technology. The simulation results exhibit a -3 dB bandwidth of 5 GHz, input-referred noise current of 17.74 pA/√Hz, and power consumption of 3.2 mW. This design approach renders the TIA input insensitive to the input photodiode, exhibiting a stable frequency response over a range of photodiode capacitance from 50 fF to 300 fF.

A linearity improved equalizers for short-channel communication links

P Singh, R Walia, R Nagulapalli, M Sakare - 35th Irish Signals and Systems Conference (ISSC), 2024

Abstract: The paper introduces a novel Continuous-Time Linear Equalizer (CTLE) circuit aimed at improving linearity by replacing conventional current sources with high-linear poly resistors. A key innovation lies in the adoption of a Voltage-to-Current (V2I) converter instead of the conventional current source in the CTLE bias circuitry. This strategic change directly targets the main sources of linearity limitations, setting this approach apart and introducing a more effective means of managing bias currents in the CTLE. The anticipated benefits of this innovative modification include a significant enhancement in circuit linearity performance and a consequent reduction in Total Harmonic Distortion (THD). The proposed CTLE has been designed using a standard 65nm CMOS technology, with a 1V power supply and an active area of 0.023mm ^{2}. The post-layout simulation results confirm that the CTLE operates correctly. It demonstrates

	superior performance for a 12-inch channel at a data rate of 12.5 Gb/s, with an eye width of 71.24 ps, an eye height of 98.82mV, and a jitter of 8.63 ps. The proposed CTLE consumes 3.29mW, exhibiting a FoM of 0.26 p $^{J/b}$. These advancements in the CTLE module represent significant progress in optical circuit innovation, signalling a meaningful stride toward achieving enhanced performance and reliability in modern circuit designs
16.	A noise and mismatch improved charge pump for PLL in 28nm CMOS technology **H Mehra, MK Singh, ZR Sheikh,** R Nagulapalli, **M Sakare -** 2024 International Conference on Integrated Circuits, Communication, and Computing Systems (ICIC3S), 2024 **Abstract:** Conventional H-bridge charge pump (Hcp) is a well-known architecture for type-2 Phase-Locked-Loop (PLL) applications. However, this has significant noise and mismatch due to random variation of CMOS devices. Replica-assisted HCP will improve the mismatch due to VDS mismatch, but it can't improve the random mismatch. In this paper, a resistor-based Charge Pump (CP), which produces the CP current by using a voltage-to-current converter (V to I converter), has been proposed. This will improve the mismatch sensitivity and thermal noise due to the inherent mismatch performance of the resistor. The proposed resistor-based CP has been designed to produce $120\upmu\ \mathrm{A}$ current for a 1 MHz Bandwidth type-II PLL application in 28 nm CMOS technology. The postsimulation results show 0.8 % mismatch (sigma) and thermal noise at 1 MHz frequency. The mismatch performance is 1.89x better than the existing one while checking on 200 Monte Carlo (MC) simulations. This consumes $120\upmu\ \mathrm{W}$ power from a 1 V nominal supply and occupies an area of $15200\ \upmu^{2}$ silicon area, including decoupling capacitors.
17.	A spectro-statistical approach for emotion identification from EEG signals **LR Sookha, G Sharma, MA Ganaie, A Dhall** - IEEE 18th International Conference on Automatic Face and Gesture Recognition (FG), 2024 **Abstract:** Automatic identification of emotions is important in human-centered computing. It allows machines to better understand user emotions. Identifying emotions via neural sensing techniques such as electroencephalogram (EEG) is a promising approach. In this paper, we aim to identify the emotions class from EEG signals. We frame emotion identification as a classification task and apply spectral and statistical encoders to extract the relevant features. We validate our approach on EmoNeuroDB dataset. Our method outperforms the EmoNeuroDB baseline, achieving a 42.10% increase in class prediction accuracy.
18.	An investigation on mechanical and electrochemical properties of Ti-6Al-4V alloy by scheduling heat-treatment in pure β and α+ β region BP Mahto, **D Singh, R Kumar**, RK Rai, MK Mishra - International Conference on Fundamental and Industrial Research in Materials (iConFIRM- 2023), 2024 **Abstract:** The present study investigates the effect of various heat treatments on the microstructure, mechanical properties, and electrochemical behavior of Ti-6Al-4V alloy. The heat treatment (HT) comprises of treating above and below beta transus temperature (T$_β$) followed by aging at 650 ℃ for 2 h and furnace cooling. Results reveal that heat treatment temperature and cooling rate significantly modify the microstructure, mechanical, and electrochemical behaviour. Notably, the beta quenched and aged sample (HT-1) exhibited the highest tensile strength (1166 MPa) possibly due to the formation of α′ martensite. On the other hand, the microstructure of the beta annealed and aged sample (HT-2) consists of Widmanstatten α/β phase. Conversely, the microstructure of the solution treated sample (HT-3) contains globular primary α$_P$ and acicular α′, which resulted in balanced mechanical properties (tensile strength of 1124 MPa and 18% elongation). Duplex annealed sample (HT-4) exhibits globular α$_P$ and Widmanstatten α/β phase. Furthermore, it is seen that the best corrosion resistance is observed during HT-1 condition. Research findings show crucial insights into tailoring the microstructure, mechanical, and electrochemical properties of Ti-6Al-4V alloy through precise heat treatment.

19.	An IoT-Based Biodiversity Monitoring System **R Verma, R Raina, V Garg, S Gautam, S Kumar** - 2024 IEEE International Conference on Omni-layer Intelligent Systems (COINS), 2024 **Abstract:** In order to monitor the health of beehives and understand bee behavior effectively, there's a pressing need for thorough data collection and transmission. This paper proposes an IoT-based system architecture designed to facilitate real-time data gathering and transmission for remote monitoring of beehives. The system utilizes MQTT and HTTP IoT messaging protocols to send various data metrics such as temperature, humidity, light intensity, insect count, frame, and video data from a biodiversity sensing node to the cloud. Additionally, the paper outlines the structure of the messages used for transmitting this data for a clearer comprehension. Field experiments were conducted to evaluate the performance of different Quality of Service (QoS) levels for MQTT data delivery and video transmission via HTTP. By providing real-time data, this system aims to enhance the study of bee activities and contribute to the development of precise beekeeping techniques.
20.	An RC-based dual injection locked delay cell for high-frequency ring VCOs **MK Singh,** R Nagulapalli, **DM Das, M Sakare** - 35th Irish Signals and Systems Conference (ISSC), 2024 **Abstract:** This paper proposes an RC-based dual injection-locked (RC-DIL) delay cell for a coupled ring voltage-controlled oscillator (RVCO). The RC-DIL delay cell uses an RC network instead of PMOS cross-coupled architecture. It reduces the power dissipation of the delay cell and the overall RVCO. The RC-DIL delay cell employs two NMOS transistors for injection lock, a technique utilized to generate a poly-phase response within the RVCO, and for coupling two RVCOs to maximize the operating frequency range. This RC-DIL delay cell further improves the operating frequency because of the extra discharging path from the RVCO's output node, which reduces the discharging time. The post-layout and Monte Carlo simulations of the RC-DIL delay cell-based RVCO are performed in 65 nm CMOS technology using 1 V supply. The power dissipation and the phase noise of the RC-DIL delay cell-based RVCO is 3.6mW and -96.6 dBc/Hz at 1 MHz offset frequency. The power dissipation is improved by 63.8% in RC-DIL delay cell-based RVCO compared to conventional RVCO. The figure of merits (FoMs) i.e. FoM_1, FoM_T (including tuning range), and FoM_N (including the number of phases) of RC-DIL delay cell-based RVCO, are - 160.2 dBc/Hz, -174.5 dBc/Hz, and -185.2 dBc/Hz which are 5.9 dB, 15.1 dB, and 14 dB better than conventional RVCO.
21.	Anomaly detection across multiple farms through remote sensing **H Bodkhe, H Raj, D Kumar, N Wadhavinde, N Goel, M Saini** - International Conference on Computer Vision and Image Processing (CVIP- 2023), 2024 **Abstract:** In effective agricultural management, monitoring crop growth is crucial. Various factors, including climate, pests, diseases, and soil variations, can lead to abnormal yields. Detecting anomalies, where one farm's growth deviates from its neighbors with similar crops and sowing dates, can help identify early signs of crop diseases. Remote sensing technologies, like satellites and drones, provide real-time crop growth information, enabling informed decisions for farmers. This paper presents a satellite-based anomaly detection technique. We extract NDVI values, sowing dates, and current dates for each farm, normalize the data, and employ the DBSCAN algorithm to detect anomalies. Our results demonstrate that DBSCAN outperforms other models with a silhouette score of 0.5369, improving crop yield prediction.
22.	Arm angle dependence of X-shaped metamaterial resonator in the X-band regime S Samanta, **GP Singh,** P Jain, AK Singh, **N Sardana** - International Conference on Fundamental and Industrial Research in Materials, 2023 **Abstract:** An angle dependent tunable design of an X-shaped metamaterial resonator (MMR)

	was theoretically and experimentally investigated in X-band (8–12 GHz). Single X-shaped MMR structures made of copper were simulated by changing the angle θ (w.r.t. magnetic field axis), and the data was confirmed experimentally with a Vector Network Analyser (VNA). The results indicated that with increasing angle, the resonance frequency was shifted towards the higher frequencies. Surface current data attributes the resonance to its magnetic component. Furthermore, the effective intrinsic parameters were calculated using Nicolson-Ross-Weir (NRW) technique to verify the metamaterial behavior of the resonator. The model with $\theta = 60°$ showed the best response, with a low return loss and a high figure of merit (FOM), which can be used for X-band stealth applications and radar communications.
23.	Communication receiver design for PSK-LFM joint sensing and communication waveform **D Salwan, S Agarwal, B Kumbhani, S Darshi**… - 2024 IEEE International Conference on Communications Workshop on Emerging Technologies in Aerial and Space Networks, 2024 **Abstract:** Over the past few years, several innovations in the wireless, automation, and defence sectors have witnessed a need for jointly designing sensing and communication technologies on a single platform. This will reduce the system size and cost and solve the spectrum congestion issue. In this paper, we propose novel strategies for symbol detection at the communication receiver of an unmanned aerial vehicle (UAV) using a phase shift keying-linear frequency modulated (PSK-LFM) waveform. Radar waveform takes enormous bandwidth for better range resolution. However, processing the same waveform at the communication receiver would require high Analog-to-Digital Converter (ADC) sampling. To reduce the sampling rate, we propose two variants of the same. In one case, part of the received signal is filtered and sampled for further processing, while in the other case, the whole signal is undersampled to detect the bits. We obtain the bit error rate (BER) analytical expressions for all the cases and show that a better BER performance can be obtained even if we undersample the received signal.
24.	Efficient contextual feature network for single image super resolution **Inderjeet, JS Sahambi** - International Conference on Computer Vision and Image Processing (CVIP- 2023), 2024 **Abstract:** The field of efficient super-resolution techniques has witnessed significant progress, with advancements in reducing parameters and FLOPs and enhancing feature utilization through complex layer connections. However, these methods may not be suitable for resource-constrained devices due to their computational demands. We propose a novel approach called Efficient Contextual Feature Network (ECFN) to address this issue. ECFN utilizes two convolutional layers to learn residual contextual local features, striking a balance between model effectiveness, inference speed, and efficiency. These updates improve performance compared to previously reported efficient super-resolution models for Single Image Super-Resolution (SISR), offering faster runtime without compromising high PSNR or SSIM.
25.	Finite element modelling in bones: A review **K Singh, A Tiwari** - 2023 International Conference on Fundamental and Industrial Research in Materials, 2024 **Abstract:** This review explores the utilization of Finite Element Method (FEM) modelling in the field of bone biomechanics. It emphasizes the crucial significance of bone biomechanics within the field of medical research for therapeutic applications. The versatility of finite element method (FEM) is demonstrated in its application to biomechanical investigations, clinical applications, and disease modelling. Nevertheless, this study also acknowledges and discusses the obstacles and potential avenues for further exploration within the discipline. The discussion revolves around the careful management of model complexity and computing efficiency, the need for accurate material characterization, the importance of interdisciplinary collaboration, and the ethical considerations involved. In its whole, the review illustrates the significant role of finite element modelling (FEM) in advancement of bone biomechanics research and its practical

	applications.
26.	Influence of density on the dynamic properties of intact rock masses S Rohilla, R Sebastian - Proceedings of the Indian Geotechnical Conference(IGC- 2022), 2024 **Abstract:** The determination of dynamic properties of geomaterials is essential from the point of view of many geotechnical engineering problems subjected to dynamic loading. The density of the geomaterial plays a vital role in deciding the dynamic properties and Poisson's ratio of the material. In the present study, resonant column apparatus has been used for the laboratory testing of intact gypsum material to identify the influence of density on the dynamic properties of Poisson's ratio of rocks. The experimental results showed that the unconfined compressive strength of the material increases exponentially with increased density. The reduction in the Poisson's ratio and material damping ratio and a rise in the dynamic modulus have been observed with an increase in the density of the material. Furthermore, with the rise in the strain amplitude, the value of Poisson's ratio and damping ratio increases, and the modulus value decreases. The study attempted to establish the correlation between the density and the dynamic properties of the material under varying strain amplitudes
27.	Investigation on solid-State carbothermic reduction behaviors of Pyrolusite ore S Tripathy, NS Randhawa - International Conference on Fundamental and Industrial Research in Materials (iConFIRM- 2023), 2024 **Abstract:** Manganese is essential to iron and steel production because of its sulfur-fixing, deoxidising, and alloying properties. Also, manganese has no satisfactory substitute in producing aluminium alloys and battery cells. It was estimated that manganese ore consumption reached about 200 million metric tons in the last decade. The most important manganese ore is pyrolusite (MnO_2), which is composed of higher manganese oxide and needs more energy to obtain manganese metal. Previous studies suggest that pre-reduced ore pellets in FeMn production lead to a significant drop from ~3000 to ~1600 kWh t^{-1} in energy consumption. Hence, the prereduction of manganese ores is essential to increasing ferromanganese production efficiency and cost-effectiveness. This study analysed the kinetics and mechanism of roasting of pyrolusite manganese ore for use in ferromanganese production. Mixtures of ore-coke in a ratio of 1:0.15 were prepared for carbothermic reduction. The effect of ore sizes (5–20 mm), reduction temperatures (900–1100 °C) and holding time (60–180 min) on the reduction behaviour were examined. Optimum conditions were obtained for a higher reduction of ore. The decomposition of higher oxide states of manganese was confirmed from XRD analysis of raw and reduced ores. Our study indicated that the reduction of the ore was inversely dependent on its size, whereas a higher temperature and the holding time improved the reduction of the ore.
28.	Iron recovery approach from steel slag using droplet coalescence technique SS Chandel, A Maurya, NS Randhawa, PK Singh - International Conference on Fundamental and Industrial Research in Materials, 2023 **Abstract:** Currently, the world's utilization rate of steel slag is relatively low, and it is primarily used for landfills, which has a negative impact on the environment and a cost to the economy. Compared to ironmaking slags, steelmaking slag has a relatively high percentage of total iron (between 20 and 35%). The high iron content of slag is a concern for the metalworking industry. Due to the presence of micron-sized iron particles that become trapped, the recovery of iron from slag was limited. Iron entrapment during the reduction of iron oxides in slag systems is a significant issue that reduces the iron yield from the system. This study examines the iron recovery mechanism from molten slag. At the molten stage, the force of attraction between molecules of individual components varies, rendering them an immiscible fluid, particularly metallic iron due to significant difference in density. In this study, iron recovery tracking parameters such as iron agglomeration and its settling time have been examined numerically. Using the commercial CFD software Ansys Fluent, a numerical calculation was performed to

	predict the size of the metal particle, the settling velocity, and the settling time. A three-dimensional numerical simulation was established using the volume of fluid (VOF) model and slag basicity's ranging from 0.9 to 1.5. In addition, the particle orientation and equivalent droplet radius of metallic iron droplets are examined to support the mechanism and compared with real scenario.
29.	**Modeling and comparing the impact of resistive and capacitive crossbar associated parasitics of neuromorphic circuits** **SA Thomas, S Kushwaha,** R Sharma**, DM Das** - 31st International Conference on Mixed Design of Integrated Circuits and System (MIXDES), 2024 **Abstract**: Neuro-inspired computing systems have shown a promising future in artificial intelligence. To meet the performance requirement of neuro-inspired computing systems, various synaptic devices are being used to store the weights. Resistive synapses have been in focus, but recently, capacitive synapses have emerged as a potential candidate for the synaptic device. Increasing complexity in a neuromorphic system causes the interconnect parasitics to significantly affect the circuit's performance. Therefore, this paper provides a comprehensive study on how the resistive and capacitive synapse-based crossbar parasitics affect the performance of the system. To extract the parasitic components, a Q3D model is designed considering both the resistive and capacitive synapses. A complete crossbar-associated parasitics architecture is designed that can be used to analyze the crossbar of any dimension. The analysis is done to compare the parasitic effect of both the resistive and capacitive synapses on different spiking patterns of the Izhikevich neuron for different crossbar sizes. Based on the results, the capacitive synapse-based crossbar array outperforms the resistive synapse in terms of reduced signal distortion and delay. The circuit implementation is done using 180 nm standard CMOS technology.
30.	**Molecular dynamics simulations of diffusivity in an atomic scale diffusion multiple** **Jhalak, D Beniwal, PK Ray** - International Conference on Fundamental and Industrial Research in Materials (iConFIRM 2023), 2024 **Abstract:** Accurate measurement of diffusivity is critical for several diffusion-controlled materials phenomena ranging from creep to oxidation. Experimental measurements of diffusion coefficients are expensive and time-intensive, especially while using diffusion couples. To an extent, the measurements are expedited using diffusion multiples. Ab-initio methods, within the framework of the Nudged-Elastic Band method as well as Molecular Dynamics (MD) can be employed for modeling diffusion. However, the traditional diffusion couple approach makes this time-consuming as well. Here, we adopt classical MD for creating an experimental analogue of diffusion multiples and demonstrate the concept using a ternary diffusion multiple consisting of Ti, Ni and V and assess the interdiffusion coefficients across Ti-Ni, Ti-V and Ni-V interfaces.
31.	**Numerical simulation study on detection of subsurface micro crack using active infrared thermography** **M Jaiswal, R Sebastian**, R Mulaveesala - Proceedings of the Indian Geotechnical Conference (IGC- 2022), 2024 **Abstract:** Bursting of brittle rock is an abrupt and violent phenomena of rock failure in high stress mines that result in many irreparable losses, including human lives. In general, large number of microcracks initiation and propagation in rocks lead to the spalling of rocks in underground construction, therefore detection of microcracks and location of its amalgamation help to adjudge the stability and to give the early warning indications. A simulation study has been carried out using FEM software to examine the potential of subsurface microcracks detection using pulse infrared (IR) thermography. Using this proposed method, the potential collapse location along with crack depth and size of rock can be estimated. A box-shaped granite rock with artificially planted microcracks of different width and depth has been geometrically

	modelled. A 3D convective heat transfer equation along with coded pulse input has been used to check the detection potential. A phase mechanism was adopted for extracting the features based on fast Fourier transform technique using MATLAB code. Further, single-pixel temperature profiles at the surface of sound zone and cracked zone of the test samples were compared. The proposed predictive analysis may help to reduce the casualty that is caused by rock burst.
32.	[Prediction of chiller thermal characteristics in radiant cooling systems](#) G Singh, S Deb, R Das - 2024 International Conference on Signal Processing, Computation, Electronics, Power and Telecommunication (IConSCEPT), 2024 **Abstract:** This study is intended to develop an artificial-neural-network (ANN)-based model that computes the necessary chiller thermal energy/heat transfer rate in a desiccant and sensible heat recovery wheel integrated vapor absorption-based radiant cooling system (RCS). Solar and natural gas were the main energy sources. The RCS was installed with a 4-floor corporate building of 4998 m2 . By applying the time-variant weather data, radiant and dedicated outdoor air system (DOAS) chiller capacities of the RCS may be pre-determined securely in a more convenient manner. During the development, the ANN structure was fed with input neurons containing solar irradiance, outdoor temperature, and moisture contents. These had statistical connection with the output neuron denoting radiant and DOAS chiller heat transfer rates. The entire ANN framework was optimized for the analysis and the parametric predictions. Results were studied using mean-squared error, correlation coefficient (R), and error histograms. For heat transfer rate predictions of radiant and DOAS chillers, R values were determined above 86% and 95%, respectively. Finally, histograms exhibited that for most of the samples, errors of 0.0025 and 0.03366 were involved with parametric predictions of radiant and DOAS chillers, respectively. Therefore, the presented ANN was proven to have the capability to be implemented in sustainable energy-based building designs.
33.	[Probing NV center coupled metal-dielectric-metal architectures for quantum technologies](#) N Singh, D Sehgal, A Venkatesan, RV Nair - Quantum 2.0 Conference and Exhibition, 2024 **Abstract:** We experimentally demonstrated the emission rate and intensity enhancement of NV centers mediated by metal-dielectric-metal cavity coupling. Results show the wide tunability of cavity mode, a vital platform for coupling various quantum emitters.
34.	[Speeding up government procurement workflows with LLMs](#) A Sofat, B Sodhi - 13th International Conference on Electronic Government and the Information Systems Perspective (EGOVIS), 2024 **Abstract:** Public procurement requires careful preparation of tender documents that must comply with regulatory requirements and the tendered items' specifications. Later, when the bids are received, they need to be diligently evaluated for compliance. All these steps involve significant manual effort from the subject matter experts (SME). The bid evaluation alone takes several days to complete, often leading to delays and cost overruns. We present a system design that leverages LLMs to significantly reduce the bid analysis and evaluation effort. Traditional methods often struggle with extracting nuanced information and understanding complex relationships within bid documents. Our proposed system addresses these challenges by integrating LLMs for contextual understanding and retrieval-augmented generation for precise query answering. We present a comprehensive system design, highlighting its innovative features and potential for advancing information analysis tasks in tender bid evaluation. We have evaluated our system on diverse tenders data available through Indian e-procurement portals [2]. Our experiments show that our system is able to reduce the bid compliance check time from hours to seconds.
35.	[Sustainability assessment of MICP for ground improvement](#) M Sharma - Proceedings of International Conference on Environmental Geotechnology, Recycled Waste Materials and Sustainable Engineering (EGRWSE), 2024

	Abstract: Microbially Induced Calcite Precipitation (MICP) is a promising ground improvement technique that has attracted meaningful consideration recently, because of its potential to enhance soil properties and reduce the environmental impact of conventional soil stabilization techniques. However, the sustainability of this technique needs to be evaluated in terms of economic, environmental, and social factors. Economically, the cost-effectiveness of MICP needs to be assessed, taking into consideration the initial investment, maintenance, and long-term benefits of the technique. Environmental sustainability needs to be evaluated by analyzing the carbon footprint and other environmental impacts of the process. Also, the feasibility of using locally available materials for the process needs to be assessed to reduce the environmental impact of transportation and associated carbon emissions. Social sustainability needs to be assessed in terms of the potential health risks associated with the use of microbial agents, as well as the impact of the process on local communities. A comprehensive sustainability assessment should also consider the ethical implications of using biotechnology for ground improvement purposes. Hence, the sustainability assessment of MICP for ground improvement requires a multi-disciplinary approach that considers, economic, environmental, and social factors. The results of such an assessment can help in developing sustainable and resilient solutions for ground improvement.
36.	The effect of phase-matching on OAM entanglement in high-gain SPDC Y Xu, L Niu, **G Kulkarni**, RW Boyd - Proceedings Volume 13106, Photonics for Quantum, 2024 **Abstract:** Recent progress in the study of the non-classical macroscopic state of light sheds light on the characterization of high-gain spontaneous parametric down-conversion (SPDC). However, the theory of high-dimensional entangled photon pairs with SPDC in this high-gain regime is far from being complete. Here, we present a numerical study of the effect of the phase-matching function on the OAM entanglement in high-gain SPDC. We use a recently developed classical model of high-gain SPDC to compute the OAM spectrum of the entangled photon pair and examine how the OAM entanglement depends on various physical parameters determining the phase-matching function. Our study offers guidelines for quantum state engineering with bright sources of photon pairs entangled in high-dimensional OAM spaces.
C	**Editorial(s)**
37.	Role of non-coding RNAs (emphasis on the emerging role of circular RNAs) in cancer: Application potential for molecular diagnostics and therapeutics of cancer S Naidu, S Karnati, H Radhakrishnan, A Gupta - Frontiers in Genetics, 2024 **Abstract:** Amidst the intricate genetic landscape of the human genome, a diverse array of non-coding RNAs (ncRNAs) has emerged as critical regulators of gene expression and cellular function (Nemeth et al., 2024). Among these, circular RNAs (circRNAs), microRNAs (miRNAs), and long non-coding RNAs (lncRNAs) form essential components of regulatory networks that govern cell fate in both normal and pathological contexts (Loganathan and Doss, 2023). There is substantial evidence that dysregulation of these ncRNAs is a hallmark of cancer. Notably, their distinct expression profiles hold immense potential for diagnosis, prognosis, and therapy, opening new avenues for molecular diagnostics and combinatorial treatments (Uppaluri et al., 2023). This editorial summarizes five high-impact review articles that delve into the pivotal advancements of ncRNAs in cancer research, addressing critical aspects of molecular oncology.
D	**Journal Article(s)**
38.	A comprehensive review on failure aspects of additive manufacturing components under different loading conditions R Yadav, SS Yadav, **R Dhiman**, R Patel - Journal of Failure Analysis and Prevention, 2024

Abstract: Understanding the underlying cause of the failure mechanisms of additive manufacturing (AM) components is essential for developing fatigue-resistant materials and improving the performance of AM components. This comprehensive review article discusses the mechanical failures of AM components including tensile, fatigue, and fracture, which arise due to microstructural heterogeneity influenced by various factors such as porosity, lack of fusion, thermal gradient, powder characteristics, and bonding mechanism. The article also explores the optimization of processing parameters such as beam size, power, temperature, and material deposition rate to enhance resistance against these failures. Additionally, it discusses the various post-processing techniques to mitigate the defects-related issues of additive manufacturing processes, and finally, future research perspectives are pointed out. The comprehensive review contributes to understanding the mechanical and microstructural aspects of the failure mechanisms of the AM components.

39.	Algorithmic results for weak Roman domination problem in graphs **K Paul, A Sharma, A Pandey** - Discrete Applied Mathematics, 2024 **Abstract:** Consider a graph G=(V,E) and a function f:V→{0,1,2}. A vertex u with f(u)=0 is defined as undefended by f if it lacks adjacency to any vertex with a positive f-value. The function f is said to be a weak Roman dominating function (WRD function) if, for every vertex u with f(u)=0, there exists a neighbor v of u with f(v)>0 and a new function f$'$:V→{0,1,2} defined in the following way: f$'$(u)=1, f$'$(v)=f(v)−1, and f$'$(w)=f(w), for all vertices w in V\\{u,v}; so that no vertices are undefended by f$'$. The total weight of f is equal to $\sum_{v \in V} f(v)$, and is denoted as w(f). The Weak Roman domination number denoted by γ_r(G), represents min{w(f)|fis a WRD function ofG}. For a given graph G, the problem of finding a WRD function of weight γ_r(G) is defined as the Minimum Weak Roman domination problem. The problem is already known to be NP-hard for bipartite and chordal graphs. In this paper, we further study the algorithmic complexity of the problem. We prove the NP-hardness of the problem for star convex bipartite graphs and comb convex bipartite graphs, which are subclasses of bipartite graphs. In addition, we show that for the bounded degree star convex bipartite graphs, the problem is efficiently solvable. We also prove the NP-hardness of the problem for split graphs, a subclass of chordal graphs. On the positive side, we present a polynomial-time algorithm to solve the problem for P_4-sparse graphs. Further, we have presented some approximation results.
40.	An ensemble model health care monitoring system **H Anumala** - Critical Reviews™ in Biomedical Engineering, 2024 **Abstract:** Internet of things (IoT) is utilized to enhance conventional health care systems in several ways, including patient's disease monitoring. The data gathered by IoT devices is very beneficial to medical facilities and patients. The data needs to be secured against unauthorized modifications because of security and privacy concerns. Conversely, a variety of procedures are offered by block chain technology to safeguard data against modifications. Block chain-based IoT-based health care monitoring is thus a fascinating technical advancement that may aid in easing security and privacy problems associated withthe collection of data during patient monitoring. In this work, we present an ensemble classification-based monitoring system with a block-chain as the foundation for an IoT health care model. Initially, data generation is done by considering the diseases including chronic obstructive pulmonary disease (COPD), lung cancer, and heart disease. The IoT health care data is then preprocessed using enhanced scalar normalization. The preprocessed data was used to extract features such as mutual information (MI), statistical features, adjusted entropy, and raw features. The total classified result is obtained by averaging deep maxout, improved deep convolutional network (IDCNN), and deep belief network (DBN) ensemble classification. Finally, decision-making is done by doctors to suggest treatment based on the classified results from the ensemble classifier. The ensemble model scored the greatest accuracy (95.56%) with accurate disease classification at a learning percentage of 60% compared to traditional classifiers such as neural network (NN) (89.08%),

|	
	long short term memory (LSTM) (80.63%), deep belief network (DBN) (79.78%) and GT based BSS algorithm (89.08%).
41.	Analytic Kramer sampling and quasi lagrange-type interpolation in vector valued RKHS **S Mahapatra, S Sarkar** - Results in Mathematics, 2024 **Abstract**: This paper discusses an abstract Kramer sampling theorem for functions within a reproducing kernel Hilbert space (RKHS) of vector valued holomorphic functions. Additionally, we extend the concept of quasi Lagrange-type interpolation for functions within a RKHS of vector valued entire functions. The dependence of having quasi Lagrange-type interpolation on an invariance condition under the generalized backward shift operator has also been discussed. Furthermore, the paper establishes the connection between quasi Lagrange-type interpolation, operator of multiplication by the independent variable, and de Branges spaces of vector valued entire functions
42.	Analytically pricing European options in dynamic markets: Incorporating liquidity variations and economic cycles XJ He, **P Pasricha**, S Lin - Economic Modelling, 2024 **Abstract:** This paper discusses the European option pricing problem in the context of asset prices being influenced by liquidity risks and economic cycles. We employ regime switching for asset volatility, and liquidity risks are captured by market-wide liquidity. We obtain an analytical formulation of European option prices, allowing for fast model calibration using real-market data. By estimating model parameters using real option data, we show that pricing errors can be significantly reduced using our model that considers stochastic liquidity, indicating that our model has real-world applications. Our results can help investors and regulators better understand the market and provide a potentially effective risk management tool.
43.	BLE Periodic advertising based energy efficient sensor node operation for transfer of large data in monitoring applications **S Gautam, S Kumar** - IEEE Internet of Things Journal, 2024 **Abstract:** IoT applications like livestock and personalised health care monitoring systems have large amounts of data obtained per second from sensors interfaced to battery operated sensor nodes. In such networks, all the data generated at the nodes must be successfully sent to the central receiving device ensuring minimal power consumption of the data transmission operation, to enable longer lifetimes of battery-operated sensor nodes. In this paper, in order to minimize energy consumption of sensor nodes, we propose a Bluetooth Low Energy (BLE) based data transfer approach relying on BLE periodic advertisements, which allow up to 255 bytes of payload to be sent in one packet and minimize the involvement of interference prone primary advertising channels in the data transfer process. By using primary channel transmissions only for one-time device discovery and then disabling them, the proposed technique ensures that number of transmissions made by each sensor node for successful data delivery in large sensor networks is reduced in comparison with conventional extended and periodic advertisements. This offers reduction in energy consumption of sensor nodes due to reduction in radio on time. Through extensive real-time and simulation-based experimentation conducted, we have shown that, in a network of 200 sensor nodes, the proposed periodic advertising based technique requires much lesser radio on time for reliable data delivery and reduces energy consumption of the sensor nodes by almost 51% and 20% as compared to the consumption when extended and standardized periodic advertisements are used to communicate the data, respectively.
44.	Ceria nanoparticles immobilized with self-assembling peptide for biocatalytic applications **M Halder, V Chawla, Y Singh -** Nanoscale, 2024 **Abstract:** Peptide-based artificial enzymes exhibit structure and catalytic mechanisms comparable to natural enzymes but they suffer from limited reusability due to their existence in

homogenous solutions. Immobilization of self-assembling peptides on the surface of nanoparticles can be used to overcome limitations associated with artificial enzymes. A high, local density of peptides can be obtained on nanoparticles to exert cooperative or synergistic effects, resulting in an accelerated rate of reaction, distinct catalytic properties, and excellent biocompatibility. In this work, we have immobilized a branched, self-assembled, and nanofibrous catalytic peptide, (C12-SHD)2KK(Alloc)-NH2, onto thiolated ceria nanoparticles to generate a heterogeneous catalyst with an enhanced number of catalytic sites. This artificial enzyme mimics the activities of esterase, phosphatase, and haloperoxidase enzymes and the catalytic efficiency remains nearly unaltered when reused. The enzyme-mimicking property is investigated for pesticide detection, bone regeneration, and antibiofouling applications. Overall, this work presents a facile approach to develop a multifunctional heterogeneous biocatalyst that addresses the challenges associated with unstable peptide-based homogeneous catalysts and, thus, shows a strong potential for industrial applications.

| 45. | Cover feature: Photoredox catalysis by 21-thiaporphyrins: A green and efficient approach for C−N Borylation and C− H Arylation (Chem. Eur. J. 46/2024)
A Janaagal, A Kushwaha, P Jhaldiyal, **TJ Dhilip Kumar**… - Chemistry: A European Journal, 2024

Abstract: Transition-metal-free photoredox catalysis was used for C−N borylation and C−H arylation with 0.1 mol % loading of 21-thiaporphyrin. Under blue light, a thiaporphyrin catalyst was employed for the synthesis of boronic esters and hetero-biaryl moieties having furan, thiophene or pyrrole. The methodology was also extended to synthesize diphenyl selenide and diphenyl sulfide derivatives.

 |

| 46. | Damping the jump of coalescing droplets through substrate compliance
GC Pal, M Agrawal, SS Siddhartha, CS Sharma - Soft Matter, 2024

Abstract: Sessile droplets coalescing on superhydrophobic surfaces result in spontaneous droplet jumping. Here, through coalescence experiments and fluid–structure interaction simulations for microliter droplets, we demonstrate that such droplet jumping can be damped if the underlying substrate is designed to be compliant. We show that a compliant superhydrophobic substrate with synergistic combinations of low stiffness and inertia deforms rapidly during the coalescence process to minimize the substrate reaction, thus diminishing the jumping velocity. A spring-mass system model for coalescing water droplets is proposed that successfully captures droplet motion and substrate deformation for a wide range of compliant superhydrophobic substrates. These insights can be leveraged to improve the process efficiency in multiple applications, such as designing compliant superhydrophobic substrates for minimizing the scattering of small, nanoliter-sized droplets during atmospheric water harvesting. Lastly, experiments on an exemplar butterfly wing show that droplet jumping velocity reduction can also manifest on natural superhydrophobic substrates due to their inherent compliance. |

| 47. | Detection of soil moisture variations with fusion-based change detection algorithm for MODIS and SCATSAT-1 datasets
R Kaur, **RK Tiwari**, R Maini - Journal of the Indian Society of Remote Sensing, 2024

Abstract: Soil moisture is a vital parameter in the study of hydrology, agriculture and meteorology. The estimation of soil moisture is important for crop yield estimation, crop growth analysis and water resource management. Remote sensing is a significant way of mapping and |

monitoring crop fields' soil moisture content globally, using optical and microwave satellite datasets. In previous literature, many attempts have been made to compute soil moisture using optical and microwave-based remote sensing datasets. However, the applicability of optical data is limited due to the presence of atmospheric/cloud effects, while microwave applications are restricted due to limited resolution. In this article, a fusion-based change detection approach has been proposed to detect the soil moisture variation with multispectral and microwave satellite datasets. This study has been conducted in three stages i.e., (a) image-fusion of moderate resolution imaging spectroradiometer (MODIS) and scatterometer satellite (SCATSAT-1) at HH and VV polarization using different fusion algorithms i.e., nearest neighbour-based fusion (NNF), Gram–Schmidt (GS), Brovey transformation (BT) and principal component (PC) spectral; (b) Neural Net based classification of fused datasets to deliver the thematic maps, and (c) perform the post-classification change detection (PCD) to develop the change maps. The classified and change maps have been further utilized to detect the level of soil moisture. From the experimental outputs, it has been evaluated that the NNF-based PCD performed well enough in the development of the change maps as compared to other methods i.e., GD, BT and PC spectral. The present work can aid crop yield estimation, agricultural water and precision irrigation management.

Determination of cyclic air-fuel ratio and analysis of low and high-frequency variations in dual-fuel RCCI engine

M Saxena, RK Maurya - International Journal of Engine Research, 2024

Abstract: Higher cyclic variations (CVs) in the engine affect the performance, emissions and drivability of the vehicle. Higher CVs are one of the challenges in dual-fuel reactivity-controlled compression ignition (RCCI) engines, mainly at lower loads. Cyclic disparities in the charge preparation, such as air-fuel ratio (AFR), result in CVs in the combustion parameters. The pressure moment method (PMM) is employed in the gasoline/methanol-diesel RCCI engine to estimate cyclic disparities in AFR. The logged cyclic in-cylinder pressure is used to calculate the cyclic *AFR*. After determining the cyclic *AFR*, statistical analysis and return maps are applied for the analyses of variations in the *AFR*, CA_{10}, CA_{50}, p_{max} and IMEP. For examining the low and high-frequency disparities in cyclic AFR and its relationship with CA_{10}, Wavelet transform (WT) is further applied. A good relationship is found between the estimated mean *AFR* and the experimental mean *AFR*. Return maps signify that for the earlier start of injection (SOI), the data points of *AFR* are more scattered correspondingly, the data points for CA_{10}, CA_{50}, p_{max} and IMEP are more scattered. WT analysis shows that both high-frequency and low-frequency variations are present in dual-fuel RCCI combustion. It is found that high-frequency discrepancies in the *AFR* are consistent throughout the engine cycles for all the tested injection timings. Wavelet results confirm that high-frequency fluctuations in *AFR* result in disparities in CA_{10} and IMEP.

Effect of background noise characteristics on early warning indicators of thermoacoustic instability

N Vishnoi, L Kabiraj - Combustion and Flame, 2024

Abstract: In this work, we investigate the effects of background noise characteristics — specifically noise color (or correlation time) and intensity — arising from velocity-coupled and additive noise sources, on the early warning indicators (EWIs) of thermoacoustic instability. We employ a nonlinear reduced-order combustion dynamics model for our investigation. In the absence of noise, the nonlinear model undergoes a subcritical Hopf bifurcation, and our focus lies within the linearly stable region of the system (subthreshold region). The studied class of EWIs encompasses those derived from time series (variance), spectral analysis (coherence factor), Hurst exponent, and nonlinear methods (permutation entropy). We find that when the background noise is purely multiplicative, the trends in EWIs are primarily influenced by noise characteristics rather than the control parameter. Further, the EWIs cannot be estimated at low noise levels for large correlation times. In case of purely additive noise driven system, the

coherence factor and variance are reliable EWIs across all range of investigated noise characteristics. The Hurst exponent can serve as effective EWI when the system features large noise correlation times, while permutation entropy is effective only when the system features small noise correlation time, i.e., where white noise assumption is acceptable. When the background noise includes contributions from both multiplicative and additive sources, coherence factor and variance emerges as the most reliable EWIs. These results provide insights for selecting appropriate EWIs to be employed in practical systems, considering potential variations in noise characteristics with simultaneous changes in combustor operating conditions.

| 50. | Effect of Si content on novel medium-Mn complex phase steels |
| | **S Chand**, S Reza, **RM Prasad, K Rakha** - Transactions of the Indian Institute of Metals, 2024 |

Abstract: This investigation presents the development of third-generation advanced high-strength steels (AHSS) for automotive industries, focusing on materials with higher strength, plasticity, and crashworthiness. Three alloy steels Fe-6Mn-(1, 1.6, 2.0) Si were developed via a melting route using an arc melting furnace followed by homogenization at 1200 °C, hot rolling at 1100 °C, and then air cooling. The developed steels are characterized using FE-SEM, XRD, microhardness tester, and universal testing machine. The FE-SEM micrographs exhibit a complex phase microstructure containing pearlite, retained austenite, martensite, ferrite, and bainite. The microhardness values of novel alloys are measured as 423, 441, and 475 VHN. The tensile strengths of alloys were achieved at 1409 MPa, 1497 MPa, and 1438 MPa with elongations of 18, 15, and 14% respectively. Atom probe tomography results confirmed the presence of retained austenite of film thickness 25–27 nm. The fracture surface of alloy steel containing 1 wt% Si and 6 wt% Mn exhibits dimples, causing ductile fracture, while alloy steel containing 1.6–2.0 wt% Si and 6 wt% Mn combines dimples and facets, confirming intergranular fracture with a 14 % ductility limit. The average dimple size decreases from 0.82 μm to 0.64 μm with an increase in silicon from 1 wt% to 2 wt%.

| 51. | Elastoviscoplastic flows past a cylinder: Fluid-mechanical aspects and dynamic mode decomposition analysis |
| | **S Raffi, A Chauhan, F Hamid, C Sasmal** - Physics of Fluids, 2024 |

Abstract: When undergoing deformation, elastoviscoplastic fluids exhibit simultaneous viscous, elastic, and plastic characteristics. This study presents an extensive numerical investigation into how the combined elasticity and plasticity of such fluids influence the flow dynamics past a circular cylinder in the laminar vortex-shedding regime. By varying dimensionless numbers, such as the Weissenberg and Bingham numbers, this study elucidates their effects on various fluid-mechanical aspects, including streamlines, vorticity, drag and lift forces, and vortex-shedding frequency. The results show significant differences in the vortex street length, width, and shedding frequency downstream of the cylinder when both fluid elasticity and plasticity are present, compared to Newtonian fluids or fluids with only elasticity under the same flow conditions. Notably, flow field fluctuations are suppressed as fluid elasticity increases, an effect further accentuated by the introduction of fluid plasticity. These rheological behaviors also have a pronounced effect on the drag and lift forces acting on the cylinder. In particular, the drag forces increase with the Weissenberg and Bingham numbers while lift forces decrease. Furthermore, this study conducts the dynamic mode decomposition (DMD) analysis, a widely used reduced order modeling technique, to obtain insights into the coherent flow structures associated with the time-resolved vorticity fields for various fluids. This analysis uncovers hidden differences in the downstream vorticity structures of various fluid types using only a few DMD modes, differences that are not apparent from simple vorticity plots alone. Overall, the findings of this study are valuable for manipulating fluid-dynamical aspects, particularly the vortex-shedding phenomenon from bluff bodies, which is observed in many practical applications and natural processes.

| 52. | Engineering the functionality of Porous organic polymers (POPs) for metal/cocatalyst-free CO2 fixation at atmospheric conditions |

D Rajesh, R Kishan, D Muthukumar, RS Pillai, **CM Nagaraja** - Journal of Environmental Chemical Engineering, 2024

Abstract: Carbon dioxide (CO_2) utilization as C1 feedstock under metal/co-catalyst-free conditions facilitates the development of eco-friendly routes for mitigating atmospheric CO_2 concentration and producing value-added compounds. In this regard, herein, we designed a bifunctional porous organic polymer (POP-1) by incorporating acidic (-CONH) and CO_2-philic (-NH/N) sites by judicious choice of organic precursors. Indeed, POP-1 exhibits high heat of interaction for CO_2 (40.2 kJ/mol) and excellent catalytic performance for transforming carbon dioxide to cyclic carbonates, a high-value commodity chemical with high selectivity and yield under metal/cocatalyst/solvent-free atmospheric pressure conditions. Interestingly, an analogous polymer (POP-2) that lacks basic (-NH/N) sites showed lower CO_2 interaction energy (31.6 kJ/mol) and catalytic activity than that of POP-1. The theoretical studies further supported the superior catalytic activity of POP-1 in the absence of Lewis acidic metal and cocatalyst. Notably, POP-1 showed excellent reusability with retention of catalytic performance for multiple cycles of usage. Overall, this work presents a novel approach to metal/cocatalyst/solvent-free utilization of CO_2 under eco-friendly atmospheric pressure conditions.

53.
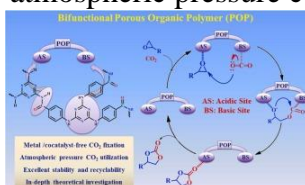
[Experimental analysis of thermal energy efficient clay brick incorporated with phase change material and insulation](#)
PKS Rathore, B Patel, **MK Gupta…** - Process Safety and Environmental Protection,2024
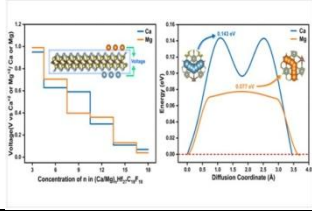
Abstract: In this study, a combination of thermal capacitance (Phase Change Material) and thermal resistance (Polyurethane Foam and air) materials are incorporated into Energy Efficient Clay Brick (EECB) to assess its indoor thermal performance. Various configurations of EECBs were developed, featuring two rectangular slots to accommodate PCM, Polyurethane Foam (PUF), and air in varying orders. These EECBs were then tested in a real outdoor tropical climate over three consecutive days to evaluate the impact of integrating PCM, PUF, and air in indoor thermal performance. The results indicate that the combination of PCM and PUF in EECB-5, with PCM on the outer side and PUF on the inner side, demonstrates the best indoor thermal behavior compared to other configurations. EECB-5 exhibits a maximum reduction in indoor peak temperature of 11.2 % and a time lag ranging from 130 to 140 minutes. EECB-5 shows a decrement factor of 0.54, followed by 0.55 for EECB-2. Additionally, EECB-5 configuration achieves an average surface temperature reduction of 15.01 % compared to Conventional Brick (CB). In addition, the simulation analysis of various configurations of bricks further confirms that the EECB-5 configuration exhibits superior indoor temperature regulation compared to other configurations. It is concluded that PCM enhances the thermal capacitance of building elements by increasing their latent heat storage capacity. Hence, Phase Change Material (PCM) into building elements can help to provide viable solutions for creating energy-efficient building envelopes.
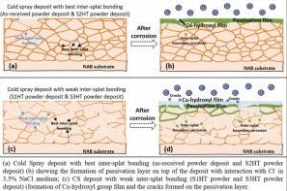

54.

[Evaluation of melting front kinetics in cylindrical phase change materials module using infrared thermography and digital imaging](#)
PJ Abass, S Muthulingam - Materials Letters, 2024

Abstract: An experimental study examined buoyancy-driven convection in the unconstrained melting of PCM within a cylindrical module. Melting progress and PCM fraction were analyzed using IRT and digital imaging. Initial symmetric melting led to accelerated phase change at the bottom and a rippled PCM surface. Thermal stratification in the lower module was evident, with

molten liquid displacing colder fluid. Observations underestimated bottom PCM waviness and melting. As the melt zone expanded, buoyancy-driven convection intensified, speeding up melting at the top while the bottom relied more on conduction. The study details transient front positions, temperature profiles, solid PCM amounts, and melting times. Unstable fluid layers near the bottom caused waviness due to chaotic fluctuations. Nucleation rates critically impacted PCM crystallization kinetics and properties.

55.	**Fluorine-terminated MXene as an anode material for dual-ion(Ca^{2+}/Mg^{2+}) batteries with rapid diffusion mobility** RP Jadav, D Singh, **R Ahuja**, Y Sonvane - The Journal of Physical Chemistry C, 2024 **Abstract:** Discovering thin and high-ion transfer mobility electrode materials is necessary to boost the charge–discharge rate of rechargeable metal-ion batteries. The functionality of two-dimensional (2D) MXenes as anode materials is largely dependent on their surface terminal groups, and surface terminal techniques are frequently employed to enhance their charge–discharge performance. Here, we construct F-terminated Hf_3C_2, while we use the first-principles calculations to explore its potential as an anode material for rechargeable metal-ion batteries, such as Mg- and Ca-ion batteries. The metallic nature and significant structural stability of the $Hf_3C_2F_2$ monolayer found by phonon and thermal properties assessed with ab-initio molecular dynamics (AIMD) and the machine learning force field (MLFF) and the low average open-circuit voltage (OCV) of 0.591 and 0.394 V and relatively low diffusion energies of Mg^{2+} and Ca^{2+} ions of 0.077 and 0.143 eV, respectively, can help improve the battery cycle. These multivalent metal cations have very low OCV values and very modest diffusion barriers, allowing the $Hf_3C_2F_2$ monolayer to be a feasible anode material for rechargeable dual-ion batteries.
56.	**Harnessing a bis-electrophilic boronic acid lynchpin for azaborolo thiazolidine (ABT) grafting in cyclic peptides** BK Das, A Chowdhury, S Chatterjee, NM Tripathi, B Pati, S Dutta, A Bandyopadhyay - Chemical Science, 2024 **Abstract:** Chemical modifications of native peptides have significantly advanced modern drug discovery in recent decades. On this front, the installation of multitasking molecular grafts onto macrocyclic peptides offers numerous opportunities in biomedical applications. Here, we showcase a new class of borono-cyclic peptides featuring an azaborolo thiazolidine (ABT) graft, which can be readily assembled utilizing a bis-electrophilic boronic acid lynchpin while harnessing the inherent reactivity difference ($>10^3$ M^{-1} s^{-1}) between the N-terminal cysteine and backbone cysteine for rapid and highly regioselective macrocyclization (~1 h) under physiological conditions. The ABT-crosslinked peptides are fairly stable in endogenous environments, but can provide the linear diazaborine peptides *via* treatment with α-nucleophiles. This efficient peptide crosslinking protocol was further extended for regioselective bicyclizations and engineering of α-helical structures. Finally, ABT-grafted peptides were exploited in biorthogonal conjugation, leading to highly effective intracellular delivery of an apoptotic peptide (KLA) in cancer cells. The mechanism of action by which ABT-grafted KLA peptide induces apoptosis was also explored.
57.	**Hydrogen embrittlement in nickel oligocrystals: Experimentation and crystal plasticity-phase field fracture modeling** **V Singh, A Raj**, Y Charles, **DK Mahajan** - International Journal of Hydrogen Energy, 2024

Abstract: This work investigates the hydrogen embrittlement (HE) behavior of Nickel-201 alloy using experimental and numerical approaches. In experimentation, the effect of electrochemical hydrogen charging on the deformation behavior of tensile oligocrystals is investigated at different strain rates. Irrespective of the strain rate levels, all the hydrogen-charged tensile oligocrystals exhibited intergranular (IG) fracture exclusively along the random high-angle grain boundaries (RHAGBs). At the same time, no crack was observed along the coincident site lattice (CSL) Σ 3 type grain boundaries. The absence of an interconnected grain boundary network, lower stress levels, and insensitivity of H-induced IG fracture to the strain rate levels of investigated FCC oligocrystals (with low lattice hydrogen diffusion coefficient) established the insignificance of dynamic H-redistribution toward HE. In numerical simulations, a crystal plasticity-phase field fracture finite element model simulates the macroscopic tensile response and corresponding microscopic fracture evolution behavior for hydrogen-free and hydrogen-charged tensile oligocrystals. The experimental results corroborated by numerical simulations, validate that the reduction in fracture energy of RHAGBs, induced by hydrogen segregation through thermodynamic equilibrium during hydrogen charging prior to deformation, is the dominating factor governing HE.

Influence of deformation-Induced martensite on non-masing behavior of 304L stainless steel
SS Yadav, SC Roy, PC Chakraborti - Journal of Materials Engineering and Performance, 2024

Abstract: This study focuses on understanding the influence of deformation-induced martensite (DIM) on cyclic plastic deformation and non-Masing behavior of 304L stainless steel (SS). Low cycle fatigue (LCF) tests and corresponding microstructural investigations were done at ± 0.25, ± 0.6, and ± 1.0% strain amplitudes at a total strain rate of 1×10^{-3}/s. Further, numerical simulations were carried out for different martensite fractions formed during LCF loading. Depending on martensite fraction and applied strain amplitude, the development of stress/strain fields around the martensite due to deformation incompatibility between the austenite and martensite leads to the formation of deformation band-like plastic zones in austenite. The strain localization and microstructural heterogeneities increased with increased martensite fraction, leading to a change in the shape of the hysteresis loop and, subsequently, the Masing/non-Masing behavior. The fatigue life of 304L SS decreased with an increase in strain amplitude vis-à-vis increased martensite fraction. The research aims to enhance the understanding of the influence of DIM on cyclic stress–strain response, fatigue life, and the non-Masing behavior of 304L SS under LCF loading.

Influence of powder heat treatment and particle size on the corrosion performance of cold-sprayed nickel-aluminum bronze (NAB) for repair applications
G Vinay, R Kant, H Singh - Corrosion Science, 2024

Abstract: Nickel-Aluminum-Bronze powder was heat-treated to reduce martensite and segregated into three sizes for Cold Spray deposition. Heat treatment (HT) significantly increased deposition efficiency (DE) from 20 % to nearly 100 %. Mechanical properties (hardness, scratch) and electrochemical corrosion tests were conducted to evaluate inter-splat bonding. Performance tests revealed that as-received (AR) powder deposit exhibited superior properties, albeit with a low DE. Among HT powders, the coarser size exhibited better inter-splat bonding due to particle size and surface oxide of the powder. The AR powder's enhanced performance is linked to a novel densification mechanism.

(a) Cold Spray deposit with best inter-splat bonding (as-received powder deposit and S2HT powder deposit) (b) showing the formation of passivation layer on top of the deposit with interaction with Cl⁻ in 3.5% NaCl medium; (c) CS deposit with weak inter-splat bonding (S1HT powder and S3HT powder deposit) (formation of Cu-hydroxyl group film and the cracks formed on the passivation layer.

---

60. Intuitionistic fuzzy generalized eigenvalue proximal support vector machine

A Quadir, **MA Ganaie**, M Tanveer - Neurocomputing, 2024

Abstract: Generalized eigenvalue proximal support vector machine (GEPSVM) has attracted widespread attention due to its simple architecture, rapid execution, and commendable performance. GEPSVM gives equal significance to all samples, thereby diminishing its robustness and efficacy when confronted with real-world datasets containing noise and outliers. In order to reduce the impact of noises and outliers, we propose a novel intuitionistic fuzzy generalized eigenvalue proximal support vector machine (IF-GEPSVM). The proposed IF-GEPSVM assigns the intuitionistic fuzzy score to each training sample based on its location and surroundings in the high-dimensional feature space by using a kernel function. The solution of the IF-GEPSVM optimization problem is obtained by solving a generalized eigenvalue problem. Further, we propose an intuitionistic fuzzy improved generalized eigenvalue proximal support vector machine (IF-IGEPSVM) by solving standard eigenvalue decomposition resulting in simpler optimization problems with less computation cost which leads to an efficient intuitionistic fuzzy-based model. We conduct a comprehensive evaluation of the proposed IF-GEPSVM and IF-IGEPSVM models on UCI and KEEL benchmark datasets. Moreover, to evaluate the robustness of the proposed IF-GEPSVM and IF-IGEPSVM models, label noise is introduced into some UCI and KEEL datasets. The experimental findings showcase the superior generalization performance of the proposed IF-GEPSVM and IF-IGEPSVM models when compared to the existing baseline models, both with and without label noise. Our experimental results, supported by rigorous statistical analyses, confirm the superior generalization abilities of the proposed IF-GEPSVM and IF-IGEPSVM models over the baseline models. Furthermore, we implement the proposed IF-GEPSVM and IF-IGEPSVM models on the USPS recognition dataset, yielding promising results that underscore the models' effectiveness in practical and real-world applications. The source code of the proposed IF-GEPSVM and IF-IGEPSVM models are available at https://github.com/mtanveer1/IF-GEPSVM.

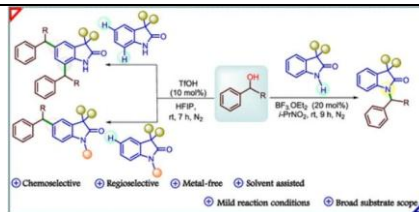|	
	Learning continuous multi-UAV controls with directed explorations for flood area coverage **A Garg, SS Jha** - Robotics and Autonomous Systems, 2024 **Abstract:** Real time on-ground information is of critical value during any natural disaster such as floods. The disaster response teams require the latest ground information of the flooded areas to effectively plan and execute rescue operations. Unmanned Aerial Vehicles (UAVs) are increasingly becoming a tool to perform quick surveys of larger areas such as flood disasters. In this paper, we propose a method to perform critical area coverage of flood-struck regions using multiple autonomous UAVs. A Deep Reinforcement Learning algorithm is proposed to learn continuous multi-UAV controls, incorporating a directed exploration strategy for the DDPG's target actor, which relies on the D-infinity (DINF) algorithm. The DINF water flow estimation technique utilizes surface elevation data to understand and predict the directed discharge of floodwater. Further, we introduce a Path scatter strategy for the multi-UAV system that inhibits the clustered formation of the UAVs over low-elevated regions. The performance of the proposed D3S (DDPG+DINF+Path Scatter) algorithm is evaluated using various performance metrics, such as average cumulative rewards, number of collisions, and UAVs' spread observed over the environment. In comparison to the baseline algorithms and other prevalent approaches in the literature, the proposed method is found to be better placed as the results highlight a significantly improved performance by D3S across different metrics.

61.

62.	Loop correction and resummation of vertex functions for a self interacting scalar field in the de Sitter spacetime S Bhattacharya, **S Kumar** - Annals of Physics, 2024 **Abstract:** We consider a massless and minimally coupled self interacting quantum scalar field theory in the inflationary de Sitter background of dimension four. The self interaction potential is taken to be either quartic, $\lambda\phi^4/4!$, or quartic plus cubic, $\lambda\phi^4/4!+\beta\phi^3/3!$ ($\lambda>0$). We compute the

four and three point vertex functions up to two loop. The purely local or partly local part of these renormalised loop corrected vertex functions grow unboundedly after sufficient number of de Sitter e-foldings, due to the appearances of secular logarithms. We focus on the purely local part of the vertex functions and attempt a resummation of them in terms of the dynamically generated mass of the scalar field at late times. Such local logarithms have sub-leading powers compared to the non-local leading ones which can be resummed via the stochastic formalism. The variation of these vertex functions are investigated with respect to the tree level couplings numerically. Since neither the secular effect, nor the dynamical generation of field mass is possible in the Minkowski spacetime, the above phenomenon has no flat spacetime analogue. We have also compared our result with the ones that could be found via the recently proposed renormalisation group techniques. All these results suggest that at late times the value of the non-perturbative vertex function should be less than the tree level coupling.

63.	[Machinability analysis of additively manufactured Ti6Al4V using micro-pillar textured tool under various cutting fluid strategies](#) **G Saraf, S Imam, CK Nirala** - Wear, 2024 **Abstract**: Additive manufacturing makes fabricating titanium alloy components directly into their near-net shapes possible, reducing the need for machining. However, post-additive manufacturing machining becomes necessary for immediate design adjustments, dimension alterations, and surface quality enhancement. The inherent thermal effects during additive manufacturing make machining challenging due to altered mechanical properties from their wrought counterpart, including increased strength and hardness with reduced ductility. Textured cutting tools are being widely used to enhance the machinability of superalloys. In this work, micro-pillar type textures, created using Reverse Micro Electrical Discharge Machining (RμEDM) on tungsten carbide inserts, aimed to explore machinability in turning operations on selective laser melted (SLM) titanium alloy. The study investigates micro-pillar interaction with SLM Ti6Al4V in chip behavior, tool morphology, cutting forces, and surface roughness under various cutting fluid strategies. Under Minimum Quantity Lubrication (MQL), textured tools show significant improvements, producing untangled chips with reduced curl radius. A considerable decrease of 38 % in the tool/chip contact area indicates a substantial reduction in the seizure zone, hence a decline in the temperature rise of the cutting tool. Dry conditions show a 20.4 % reduction in flank wear width, suggesting prolonged cutting-edge sharpness due to tool texturing. In MQL conditions, a maximum 28.9 % reduction in feed force is observed, indicating improved frictional conditions at the interface. Additionally, a 10.4 % improvement in surface finish is achieved. The work is summarized by claiming micro-pillar textured tools enhance the machinability of additively manufactured Ti6Al4V demonstrated through improvements in titanium adhesion, cutting-edge sharpness, feed force, and surface finish, particularly MQL conditions.
64.	[Metal-free switchable chemo-and regioselective alkylation of oxindoles using secondary alcohols](#) **M Lamba, PR Singh, Tanmay, A Goswami** - The Journal of Organic Chemistry, 2024 **Abstract:** In this study, we have disclosed N-alkylation and C-alkylation reactions of 2-oxindoles with secondary alcohols. Interestingly, these chemoselective reactions are tunable by changing the reaction conditions. Utilization of protic solvent and Brønsted acid catalyst afforded C-alkylation, whereas, aprotic solvent and Lewis acid catalyst afforded N-alkylation of 2-oxindoles in good to excellent yields. Regioselectivity is achieved by protecting the N-center of the oxindole and C5 alkylated product is furnished exclusively. This protocol is notable because it demonstrates functionalization at the C7 position of oxindole without the need for any directing group at the N-center. Further, a new protocol has been reported for C–H oxygenation at the benzylic position of one of the C5 alkylated derivative.

| 65.	**Microstructure, multi-scale mechanical and tribological performance of HVAF sprayed AlCoCrFeNi high-entropy alloy coating** A Meghwal, E Bosi, **A Anupam**… - Journal of Alloys and Compounds, 2024 **Abstract:** Thermal spray high-entropy alloy (HEA) coatings have demonstrated potential for improving the wear resistance of conventional materials used in extreme engineering environments. In the present work, an equiatomic AlCoCrFeNi HEA coating was manufactured using the high velocity air fuel (HVAF) process. The phase and microstructural transformations in gas-atomized (GA) powder during HVAF spraying were analyzed using SEM, EDS and EBSD techniques. The tribological properties of this HEA coating sliding against an Al_2O_3 ball at both room temperature (RT) and 600 °C were also evaluated. The GA powder was composed of Body Centred Cubic (BCC) + ordered BCC (B2) phases, which transformed to BCC + B2 + minor Face Centred Cubic (FCC) phases during the HVAF coating process, validating the thermodynamic phase prediction projected by the Scheil simulation for non-equilibrium processing conditions. The rapid solidification and high velocity impact-assisted deformation of GA powder resulted in significant grain refinement in the HVAF coating, which ultimately improved the mechanical properties at both micro and nanoscale levels. The wear resistance of the HEA coating at RT was severely impacted by the relatively brittle BCC/B2 phase structure, leading to susceptibility to abrasive wear and surface fatigue. The wear resistance at 600 °C was slightly lower at RT due to the formation of a brittle oxide layer on the worn surface, which induced surface fatigue and aggravated mass loss of the coating.
66.	**Modeling analysis, and online detection of interturn short-circuit fault in medium-frequency transformer of dual-active-bridge converter** **TJ Nistane**, S Singh, **S Payami, K Jayaraman** - IEEE Transactions on Industrial Electronics, 2024 **Abstract:** The strident working condition of the dual-active-bridge (DAB) converter has elevated the risk of interturn short-circuit fault (ITTSCF) in medium-frequency transformer (MFT). Thus, it is crucial to analyze the DAB converter under ITTSCF in MFT to avoid the complete winding short-circuit due to insulation failure. Thus, the presented work analyses the variations in the magnetizing and leakage inductance of MFT ranging from low to high severity levels of ITTSCF. Thereafter, its impact on the current stress, power transfer, and zero-voltage-switching (ZVS) of the DAB converter is presented in detail. Based on the analysis, this article presents a new reliable online ITTSCF detection technique for MFT in a DAB converter. This technique utilizes the root-mean-square (RMS) and average-based fault indices generated from the magnetizing current of MFT. The proposed fault detection technique is effective even at low severity ITTSCF (i.e., as low as 1% ITTSCF) and utilizes an off-the-shelf magnetizing current sensor to avoid extra cost. The proposed fault detection technique is immune to load variation and major switch faults in the DAB converter and thereby increases the reliability. For validation, the MFT is designed with winding taps and integrated with the hardware prototype of the DAB converter.
67.	**Modeling and tuning the electronic, mechanical and optical properties of a recently synthesized 2D polyaramid: a first principles study** M Singh, **SP Kaur**, B Chakraborty - Physical Chemistry Chemical Physics, 2024 **Abstract:** This work delves into a methodology of modeling 2D materials and their structural engineering, considering an example of a recently synthesized 2D polyaramid (2DPA-1). A

bottom-up approach similar to experimental techniques is implemented for modeling, and then its electronic structures and phonon spectrum and the quadratic nature of flexural phonons are analyzed. Furthermore, boron and nitrogen atoms are substituted for the carbon atom of the amide group of 2DPA-1, and their effects on its electronic properties, phonon spectrum, and mechanical properties are compared with those of pristine 2DPA-1 using density functional theory calculations. The *ab initio* molecular dynamics (AIMD) simulations validate the thermal stability of our system at high temperatures. The spin-polarized electronic structures reveal the transformation of pristine 2DPA-1 from a semiconductor to a half-metal and its magnetic behaviour upon nitrogen substitution. Constraining the quadratic nature of flexural phonons using the Born–Huang criteria significantly enhances the phonon spectra, leading to more accurate and reliable simulations. For modulated 2DPA-1, the elastic modulus varies between 17 and 27 N m^{-1}, and the absorption peaks shift from ~5.15 eV to 2.42 eV, enabling the application of polymeric 2D nanomaterials in photocatalysis and sensing, where light absorption in the near-infrared region is important. Finally, validation of our methodology is confirmed, as computed Young's modulus (11.26–11.76 GPa) of 2DPA-1 matches excellently with the experimental value (12.7 ± 3.8 GPa). Overall, this study reveals the modeling of a newly synthesized polymeric 2D material, and tuning its properties results in smaller bandgaps and half-metallic and magnetic behaviours.

68.

[Multi-unmanned aerial vehicle-assisted flood navigation of waterborne vehicles using deep reinforcement learning](#)
A Garg, SS Jha - Journal of Computing and Information Science in Engineering, 2024

Abstract: During disasters, such as floods, it is crucial to get real-time ground information for planning rescue and response operations. With the advent of technology, unmanned aerial vehicles (UAVs) are being deployed for real-time path planning to provide support to evacuation teams. However, their dependency on expert human pilots for command and control limits their operational capacity to the line-of-sight range. In this article, we utilize a deep reinforcement learning algorithm to autonomously control multiple UAVs for area coverage. The objective is to identify serviceable paths for safe navigation of waterborne evacuation vehicles (WBVs) to reach critical location(s) during floods. The UAVs are tasked to capture the obstacle-related data and identify shallow water regions for unrestricted motion of the WBV(s). The data gathered by UAVs is used by the minimum expansion A* (MEA*) algorithm for path planning to assist WBV(s). MEA* addresses the node expansion issue with the standard A* algorithm, by pruning the unserviceable nodes/locations based on the captured information, hence expediting the path planning process. The proposed approach, MEA*MADDPG, is compared with other prevalent techniques from the literature over simulated flood environments with moving obstacles. The results highlight the significance of the proposed model as it outperforms other techniques when compared over various performance metrics.

69.
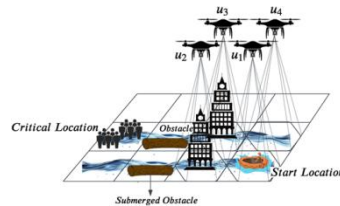
[On the effect of salt bath nitrocarburizing on the cavitation erosion behavior of AISI 304L stainless steel](#)
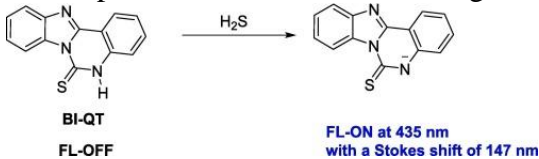**H Markanday, SC Roy**, MAJ Somers - Engineering Failure Analysis, 2024

Abstract: In this study, salt bath nitrocarburizing was applied on austenitic stainless steel AISI 304L to stabilize austenite at the surface exposed to cavitation attack. Samples were treated at 470 °C and 500 °C for 6 h, giving an average thickness of the nitrocarburized layer of 6 μm and 26 μm, respectively. The thickness of the nitrocarburized layer is found to influence the

formation of deformation-induced martensite (DIM) in the material and, thereby, the cavitation erosion resistance. The mass loss vs. time plot shows that the nitrocarburized specimens performed significantly better than the base material under ultrasonic vibratory cavitation erosion test (ASTM G32). Cross-sectional micrographs show that the phenomenon responsible for the failure in the base material is the formation of DIM. The specimen, nitrocarburized at 470 °C, showed a reduction of about 90 % in mass loss when compared to the base material (AISI 304L SS), owing to a higher yield strength (/resilience) after the formation of more stable austenite.

70.

On-resin synthesis of Lanreotide epimers and studies of their structure–activity relationships
A Chowdhury, NM Tripathi, R Jadav, V Gour, P Purohit, A Bandyopadhyay - RSC Medicinal Chemistry, 2024

Abstract: Peptide drugs often accompany epimeric impurities (isomers). Therefore, efficient chemical synthesis of epimers is critical to identify them correctly and investigate their biological activities. Here, we report the rapid synthesis and structure–activity relationship (SAR) studies of eight possible epimers of a somatostatin synthetic analog (SSA), lanreotide (LAN). SPPS and the subsequent on-resin rapid disulfide closure method offered >90% conversion yield for all epimers (P1–P8). Further, we developed an analytical method to separate these epimers, which enabled the profiling of five epimeric impurities in the API, purchased for Somatuline generic formulations. In SAR studies, most LAN epimers revealed compromised antiproliferative activity, while the P7 epimer retained antiproliferative activity similar to LAN API, as supported by in silico SAR studies in detail. Additionally, P7 showed serum stability nearly identical to LAN, suggesting that drug epimers could be a potential API. Current studies will further encourage the development of novel SSA scaffolds.

71.

Performance assessment of cold thermal storage-based building air-conditioning layouts for different climates
G Singh, R Das - Heat Transfer Engineering, 2024

Abstract: In this work, a detailed study is done to explore thermal features and operational aspects of thermal energy storage (TES)-based air-conditioning strategies. Three approaches, such as traditional air-conditioning, radiant air-conditioning unit (RACU) and desiccant-incorporated radiant air-conditioning unit (DRACU) have been undertaken by assimilating them with the TES. A validated triple-floor building with $10,690 \text{ m}^2$ floor space is studied under warm-humid, composite, and hot-dry climates. Validated strategies with TES and non-TES based techniques were then compared for exploring parametric trends defined by temperature, humidity, electricity consumption, thermal load, coefficient of performance (COP), and other aspects. In comparison with traditional non-TES strategy, results disclose that electrical energy savings offered by the TES vary between 7.6 and 11.4% for the traditional system, 4.8 and 8.6% for RACU, and 3.8 and 6.1% for DRACU, based on the subjected climate. For all of the considered systems, it is further projected that adoption of the TES although causes an increased thermal energy gain, but the same causes declination in the chiller's overall cooling load, as well as improves the net COP. Both of these factors contribute in reducing the electricity consumption. The integration of TES has revealed opposite trends for the radiant chiller attached to RACU and DRACU.

72.

Photocatalytic β-O-4 bond cleavage in lignin models and native lignin through CdS integration on titanium oxide photocatalyst under visible light irradiation
A Kumar, R Ghalta, R Bal, R Srivastava - Applied Catalysis B: Environment and Energy, 2024

Abstract: Converting lignin, a key sustainable biopolymer, into valuable oxygen-containing compounds is a significant challenge. To address such a challenge, photocatalytic self-transfer hydrogenolysis strategy is employed utilizing a $CdS(x\%)/TiO_2$ heterojunction photocatalyst, with minimal CdS loading on TiO_2. The $CdS(3\%)/TiO_2$ catalyst, under blue light, dehydrogenates

|	
	HCα–OH groups, transferring hydrogen to Cβ–O bonds, cleaving β-O-4 ether bonds in lignin model compounds yielding over 95% phenols and acetophenones. It utilizes glyceryl moieties as a hydrogen source, yielding ~ 24% of diverse lignin monomer derivatives from teak lignin. Improved charge separation in the CdS(3%)/TiO$_2$ catalyst is revealed by electrochemical and spectral analyses and exhibits delayed charge carrier recombination. Scavenging studies confirm a type II charge transfer mechanism and support visible-light-driven lignin fragmentation. The present photocatalytic process offers a promising, cost-effective approach for converting lignin into valuable aromatic compounds, advancing renewable biomass-derived chemicals.
73.	Photochemical pincer-catalyzed reductive cyclisation towards indolines and oxindoles V Singh, **N Sinha**, D Adhikari - Chemical Communications, 2024 **Abstract**: An organophotocatalytic method has been described towards the synthesis of indolines and oxindoles starting from unusual α-chloro amide and N-(2-chlorophenyl)-N-alkyl methacrylamide substrates. This marks a notable improvement since the earlier syntheses utilized iridium and gold catalysts, and involved C-I or C-Br bond cleavage as the initial step. Our photocatalyst is a pincer ligand that can be easily deprotonated to make a very strong reducing agent. The reductive cleavage of the carbon-chloride bond, and subsequent 5-exo-trig ring cyclization, followed by hydrogen atom abstraction, prepare the desired heterocycles under very mild reaction conditions. An atom economic use of KO^{t}Bu has been shown to demonstrate the unusual trifunctional role of the latter.
74.	Possible roles of phytochemicals with bioactive properties in the prevention of and recovery from COVID-19 S Koyama, PV Joseph, VDC Shields, T Heinbockel, **P Adhikari**… - Frontiers in Nutrition, 2024 **Abstract:** Introduction: There have been large geographical differences in the infection and death rates of COVID-19. Foods and beverages containing high amounts of phytochemicals with bioactive properties were suggested to prevent contracting and to facilitate recovery from COVID-19. The goal of our study was to determine the correlation of the type of foods/beverages people consumed and the risk reduction of contracting COVID-19 and the recovery from COVID-19. Methods: We developed an online survey that asked the participants whether they contracted COVID-19, their symptoms, time to recover, and their frequency of eating various types of foods/beverages. The survey was developed in 10 different languages. Results: The participants who did not contract COVID-19 consumed vegetables, herbs/spices, and fermented foods/beverages significantly more than the participants who contracted COVID-19. Among the six countries (India/Iran/Italy/Japan/Russia/Spain) with over 100 participants and high correspondence between the location of the participants and the language of the survey, in India and Japan the people who contracted COVID-19 showed significantly shorter recovery time, and greater daily intake of vegetables, herbs/spices, and fermented foods/beverages was associated with faster recovery. Conclusions: Our results suggest that phytochemical compounds included in the vegetables may have contributed in not only preventing contraction of COVID-19, but also accelerating their recovery.
75.	Purcell enhancement using spatially distributed random cavities enabled by silicon pyramid arrays **M Khokhar, N Singh, Shinki, S Sarkar, RV Nair** - Physical Review A, 2024 **Abstract:** The tailored disorder explores light-matter interaction with various functionalities in solar photovoltaic, lasing, structural coloration, and quantum technologies. However, studies are limited to exploring tailored disorder-induced light scattering, while the interactions between emitters and random cavities still need to be analyzed. We demonstrate a significant Purcell-enhanced emission using random cavities in a spatially dispersed silicon (Si) pyramid array. The numerical simulation reveals spatial confinement of electric field intensity in the cavity with substantial Purcell enhancement for an embedded emitter. We experimentally verify Purcell

	enhancement using localized emitters coupled to Si pyramids, demonstrating fivefold enhanced emission intensity. We achieve a 67% reduction in emission lifetime for random cavity-coupled emitters, which depends on Si pyramid density across the sample, supported with numerical simulations. Our results put forward an amenable approach to tailoring random cavities to manipulate the emission properties of quantum emitters.
76.	[Recycling valuable phenol from polycarbonate plastic waste via direct depolymerization and Csp2− Csp3 bond cleavage under mild conditions](#) AK Manal, DR Kanchan, A Banerjee, J Zhao, R Srivastava - ChemSusChem, 2024 **Abstract:** Upcycling plastic waste into commodity chemicals is recognized as an environmentally benign solution and beneficial for the sustained growth of humanity. Nevertheless, transition metal-free catalysts and energy-efficient conditions pose significant challenges due to the robust mechanical properties of plastics. Here, a strategy for selective production of phenol by upcycling polycarbonate waste via direct depolymerization and Csp2-Csp3 bond cleavage in an aqueous medium under mild conditions is reported. The commercial zeolites efficiently catalyze the depolymerization, Csp2-Csp3 bond hydrolysis, and direct Csp2-Csp3 bond scission at Cα of PC. Among all evaluated zeolites, HY (Si/Al=15) showed excellent catalytic performance, attributed to the ~75% yield of phenol and ~15% of acetone. The approach also employs different municipal waste PC for upcycling. Studies reveal that HY (15) exhibits high catalytic efficiency and phenol yield due to its optimum acid sites and textual properties. A scale-up experiment demonstrated that 3.1 g of phenol was produced from 5.0 g of PC, and the mass balance was 90%. A combination of control experiments, NMR analysis, and DFT studies proposed the reaction pathway. Our findings present a sustainable avenue for upcycling PC waste and offer a new way to produce phenol, contributing to the advancement of a circular economy.
77.	[Resummation of local and non-local scalar self energies via the Schwinger–Dyson equation in de Sitter spacetime](#) S Bhattacharya, N Joshi, K Roy - General Relativity and Gravitation, 2024 **Abstract:** We consider a massless and minimally coupled self interacting quantum scalar field in the inflationary de Sitter spacetime. The scalar potential is taken to be a hybrid of cubic and quartic self interactions, $V(\phi)=\lambda\phi^4/4!+\beta\phi^3/3!$ ($\lambda>0$). Compared to the earlier well studied $\beta=0$ case, the present potential has a rolling down effect due to the ϕ^3 term, along with the usual bounding effect due to the ϕ^4 term. We begin by constructing the Schwinger–Dyson equation for the scalar Feynman propagator up to two loop, at $O(\lambda)$, $O(\beta^2)$, $O(\lambda^2)$ and $O(\lambda\beta^2)$. Using this equation, we consider first the local part of the scalar self energy and compute the rest mass squared of the scalar field, dynamically generated via the late time non-perturbative secular logarithms, by resumming the daisy-like graphs. The logarithms associated here are sub-leading, compared to those associated with the non-local, leading terms. We also argue that unlike the quartic case, considering merely the one loop results for the purpose of resummation does not give us any sensible result here. We next construct the non-perturbative two particle irreducible effective action up to three loop and derive from it the Schwinger–Dyson equation once again. This equation is satisfied by the non-perturbative Feynman propagator. By series expanding this propagator, the resummed local part of the self energy is shown to yield the same dynamical mass as that of the above. We next use this equation to resum the effect of the non-local part of the scalar self energy in the Feynman propagator, and show that even though the perturbatively corrected propagator shows secular growth at late times, there exists one resummed solution which is vanishing for large spacelike separations, in qualitative agreement with the well known result found via the stochastic formalism.
78.	[Robust page object detection network for heterogeneous document images](#) HS Kawoosa, MS Kanroo, K Rana, P Goyal - International Journal on Document Analysis and Recognition (IJDAR), 2024

Abstract: Document Layout Analysis (DLA) has emerged as a challenging problem in the field of computer vision. The primary goal of DLA involves the identification of page objects including tables, figures, images, and equations from document images. In this paper, we propose a Lightweight and Robust Page Object Detection Network (LR-PODNet) for page object detection (POD) from heterogeneous document images. The proposed network improves the object detection capabilities of the YOLOv5 model by integrating the two components: Convolutional Global Attention Block (C3-AB) and Hybrid Dilated Atrous spatial pyramid pooling Block (HDAB) for POD. The C3-AB is an enhanced version of the C3 module of YOLOv5 which incorporates a global attention block instead of bottleneck-CSP block. It enhances the capability of the model to capture global dimensional features and suppresses the redundant content. The output from C3-AB is passed to the HDAB for extraction of both local and contextual features. The HDAB is strategically incorporated instead of SPPF within the YOLOv5 architecture to enhance multiple feature extraction capabilities. The experimental results show that the proposed LR-PODNet outperforms the existing methods by achieving the mAP@0.5:0.95 of 77.5% and 76.2% on the IIIT-AR-13K and NCERT5K-IITRPR datasets, respectively. Additionally, we have also evaluated the robustness of the proposed model on these two datasets by varying the IoU threshold.

79.

Role of grain size and anisotropy of neighboring grains in hydrogen-assisted intergranular fatigue crack initiation in austenitic stainless steel
A Arora, M Singh, V Nair, H Singh, DK Mahajan - Fatigue & Fracture of Engineering Materials & Structures, 2024

Abstract: This study explores the impact of microstructural features on fatigue crack initiation in poly-crystalline materials, emphasizing hydrogen-induced complexities. Grain anisotropy, misorientations, grain size variations, and elastic–plastic inhomogeneities concentrate stress at grain boundaries, making them susceptible to crack initiation during fatigue loading. The presence of hydrogen compounds this process, due to complications of characterization of local hydrogen content and activating embrittling mechanisms. Building upon a model for nickel, this research investigates 316L austenitic stainless steel specimens with varying grain sizes, both uncharged and hydrogen-charged. In situ low-cycle fatigue loading experiments establish correlations between fatigue crack initiation and microstructural features. The study reveals specific combinations of features crucial in the initiation process, undergoing alterations in the presence of hydrogen. A proposed qualitative model links microstructural features with accumulated plastic shear strain during fatigue and prevalent hydrogen embrittlement mechanisms like hydrogen-enhanced local plasticity and hydrogen-enhanced decohesion.

80.

Rotational dynamics of CNCN by p-H_2 and o-H_2 collision at interstellar temperatures
A Kushwaha, P Chahal, TJ Dhilip Kumar - The Journal of Chemical Physics, 2024

Abstract: The rotational dynamics of isocyanogen (CNCN) is studied for its collision with para (p-) and ortho (o-) hydrogen (H_2) in the temperature range of 1–100 K. These temperatures correspond to the cold dense molecular clouds in the interstellar medium where molecular hydrogen is the primary collider. An ab initio 4D potential energy surface (PES) is constructed keeping the two molecules under rigid rotor approximation. The PES is generated using the CCSD(T)-F12b/AVTZ level of theory. The 4D PES is further fitted into a neural network (NN) model, which can augment the surface and account for missing data points within spectroscopic accuracy. This NN-fitted PES is then expanded over a bispherical harmonics function to get radial terms, which are expressed into analytic functions. Thereafter, the cross sections (σ) are computed for rotational transitions of CNCN ($j \rightarrow j'$) using the close-coupling and centrifugal sudden methods for both p-H_2 ($j_c = 0$) and o-H_2 ($j_c = 1$) collision till 194 cm-1. In addition, p-H_2 ($j_c = 0, 2$) cross sections are also computed using the centrifugal sudden approximation method. The collisional rates are achieved by taking the Boltzmann distribution of σ over the translational energy of H_2 till 100 K. Finally, the CNCN–H_2 rates are compared to CNCN–He and NCCN–H_2

collisional rates. Comparing even and odd transitions for the CNCN–H_2 rates show a propensity toward higher rates for even transitions especially for o-H_2 collisions considering low-order transitions.

81.	Schlieren image velocimetry and modal decomposition study of preheated isothermal flow from a generic multi-swirl burner N Vishnoi, A Saurabh, **L Kabiraj** - Journal of Engineering for Gas Turbine and Power, 2024 **Abstract:** This study presents an experimental investigation into the turbulent flow characteristics of an unconfined counter-rotating dual swirl burner under external acoustic excitation. Utilizing Schlieren image velocimetry (SIV), we capture the velocity field of the swirling jets. Mean velocity field analysis reveals the upstream propagation of the central recirculation zone within the burner passages. Through Proper Orthogonal Decomposition (POD) analysis on instantaneous axial velocity fields, coherent structures are identified and the impact of different actuation methods on spatial modes is illustrated. Spatial modes of the unforced (natural) flow show the presence of a single and double helical Precessing vortex core (PVC) modes at St=0.53. Low-frequency acoustic actuation (St=0.46) effectively suppresses the PVC mode, while high-frequency (St=2) actuation stabilizes it. Broadband excitation of the flow field, however, induces the excitation of both single and double helical PVC modes.

82.	Simple turn-on fluorescent probe for ultrafast and highly selective detection of hydrogen sulfide in aqueous solutions SY Bong, Z Song, **K Kaur, N Singh**, YI Park, J Park, DO Jang - Spectrochimica Acta Part A: Molecular and Biomolecular Spectroscopy, 2024 **Abstract:** 5H-Benzimidazo[1,2-c]quinazoline-6-thione (BI–QT), was synthesized as a benzimidazole-based probe to detect H_2S. BI–QT exhibits a fluorescent "turn-on" response in DMSO/H_2O (9:1, HEPES 10 mM, pH 7.4) upon the addition of H_2S. The BI–QT probe can determine micromolar (0–600 µM) H_2S concentrations in aqueous systems, with a detection limit of 1.12 µM. Interestingly, BI–QT exhibited an ultrafast response to H_2S, with maximum intensity achieved almost instantly when exposed to H_2S. BI–QT is largely unaffected by pH and responds reliably over the wide 4–11 pH range, which highlights its applicability to various physiological scenarios. UV–vis, fluorescence, and ^{1}H NMR spectroscopic analyses investigated the sensing mechanism. The practicality of the probe was demonstrated using water samples and living cells. BI-QT FL-OFF H_2S FL-ON at 435 nm with a Stokes shift of 147 nm

83.	Sputter-deposited zirconium doped nickel-aluminide coatings for high-temperature oxidation-resistant applications SK Tiwari, AU Rao…**N Sardana**… - Journal of Vacuum Science & Technology, 2024 **Abstract:** Zr-Ni_3Al coatings were deposited over the Inconel-718 substrate using DC cosputtering. The deposition was carried out in a custom-designed chamber at a substrate temperature of 400 °C. The evolution of phases, microstructure, surface topography, and elemental composition were characterized using x-ray diffraction, field emission scanning electron microscopy (FESEM), atomic force microscopy, and energy dispersive spectroscopy (EDS), respectively, whereas the adhesion strength and the mechanical properties of the coatings were characterized using nanoindentation. The oxidation properties of the coatings were studied at 900, 1000, and 1100 °C in open air to determine the kinetics of oxidations. The results reveal that with the increase in Zr concentration in the host Ni_3Al matrix, the adhesive strength and mechanical properties of the films increase. The highest hardness and Young's modulus of ~9.2

|	and $\sim$150.3 GPa, respectively, are observed for 30 W Zr-Ni$_3$Al coatings. Additionally, 1.51 at. % of Zr in Ni$_3$Al coatings has shown the best oxidation resistance properties at all temperatures. However, an increase in the rate of oxidation has been observed with an increase in exposure temperature. The formation of different oxide layers after oxidation has been elucidated using FESEM and EDS after looking into the surface morphologies of the oxidized coatings.
84.	Structural credit risk models with stochastic default barriers and jump clustering using Hawkes jump-diffusion processes **P Pasricha**, D Selvamuthu, P Tardelli - OPSEARCH, 2024 **Abstract:** This paper derives a closed-form expression for the default probability and the default correlation of firms under a structural model of credit risk. Specifically, the underlying firms are assumed to have the value process driven by a Hawkes jump-diffusion model with the continuous parts of the trajectories being driven by correlated Brownian motions, while the jumps being driven by Hawkes processes having general structure of the exciting functions. The proposed framework takes into account the numerically observed facts about the default, i.e., clustering and unexpectedness. Furthermore, the default barriers are assumed to be stochastic in nature and modeled as stochastic processes, affected by common factors reflecting the systematic risk. A sensitivity analysis of default probability and correlation is conducted to investigate the impact of jump risk, clustering, and stochastic default barriers. These numerical studies demonstrate that jump clustering increases the default probability but reduces the correlation of defaults.
85.	Teaching introductory biomechanics course in low resource environment AK Tiwari, P Sinha, **J Prasad**, S Badhyal, S Joseph - International Journal of Mechanical Engineering Education, 2024 **Abstract**: Biomechanics originates at the interface of engineering mechanics and biological science. Biomechanics is an essential course for students of various disciplines, such as sports medicine, kinesiology, exercise science, orthopedics, medical sciences, biomedical engineering, and biological sciences. An introductory biomechanics course involves concepts of biology, mathematics, and mechanics that students find difficult to understand. This results in incomplete and ineffective learning of biomechanical concepts. The professional competence of a biomechanics student significantly depends on learning outcomes. Designing and developing an effective instructional methodology for an introductory biomechanics course that can improve students' learning outcomes is challenging. Teaching a biomechanics course in a low-resource environment lacking expensive biomechanics experiment equipment and commercial software is an additional challenge. Literature suggests that active learning instructional techniques can help overcome these challenges. The present study reviews active learning methods such as Experiential Learning, Problem-based Learning, Challenge-based Instructions, Just-in-Time Teaching, Game-based Learning, and Mobile Learning, which have the potential to enhance the learning outcomes of biomechanics students during an introductory biomechanics course. The present study also discusses the possibility and effectiveness of these pedagogical approaches while teaching an introductory biomechanics course in low-resource environments. A curriculum designed (lecture and laboratory modules) for effectively delivering biomechanics courses to students in low-resource environments has been suggested. This study also highlights open-source software packages and tools that are helpful for teaching and learning introductory biomechanics in low-resource settings.
86.	The merits of a folded graphene nanodevice for reliable DNA sequencing RL Kumawat, **V Shukla**, NK Jena, **R Ahuja**, B Pathak - ACS Applied Electronic Materials, 2024 **Abstract:** Inspired by controlled folding of graphene experiments, in this study, we demonstrate a folded graphene nanogap device for DNA sequencing. With the aid of first-principles density functional theory (DFT) and nonequilibrium Green's function (NEGF) based methods, we have

modeled a solid-state nanodevice comprising a folded graphene nanogap and assessed its potential for detection of four different DNA nucleotides (dAMP, dGMP, dTMP, dCMP). The electronic structure of such a working device is analyzed from the perspective of zero-bias transmission functions and the density of states for all four nucleotides. In order to characteristically distinguish the DNA nucleotides, the corresponding current–voltage (I–V) profiles have been computed, which show noteworthy distinguishable features. From our interesting findings, we have zeroed in on two voltage regimes, namely, 0.2 and 1.1 V, wherein all four DNA nucleotides manifest distinguishable current traces and make their identification plausible with better sensitivity compared to a pure graphene-based nanogap device. We have further analyzed the bias-dependent transmission function to gain a deeper understanding of the molecular and electronic states responsible for distinguishable trends in the current profiles. Our conceptualized folded graphene based nanodevice stands superior to a typical graphene nanoelectrode based device that suffers from reactivity and stability issues. Based on all these important findings, we propose a folded graphene nanogap device to be a reliable, rapid, and robust setup for fast DNA sequencing.

87.
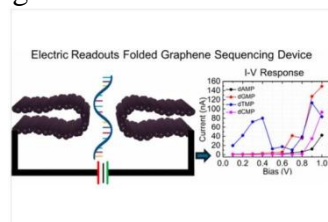
Unveiling the photocatalytic characteristics of Tl2S2 and Janus XTlS2 (X= Al, Ga, In) through first-principles analysis: Role of alternative atomic configurations
A Chafai, S Bouhou, I Essaoudi, **R Ahuja**… - International Journal of Hydrogen Energy, 2024

Abstract: In recent years, there has been increasing focus on two-dimensional (2D) materials, especially those derived from chalcogenides, due to their distinctive electrical and mechanical properties, which are crucial for numerous applications, particularly in the field of photocatalysis. Recent studies have concentrated on 2D Janus structures, investigating architectures where layers of Group-13 elements (Ga, In, and Tl) are interleaved between layers of chalcogen atoms (S, Se, and Te). Our research specifically examines the effects of swapping the positions of Group-13 and chalcogen atoms within Tl_2S_2 and Janus $XTlS_2$ (X= Al, Ga, In), emphasizing their potential as catalysts for hydrogen production through photocatalysis. Detailed analyses of the structural, optical, and electronic properties of these nanosheets were provided to elucidate their role in enhancing photocatalytic efficiency. The findings reveal the presence of covalent bonding between the two inner layers in all the compounds studied. Band structure analysis indicates that these systems are semiconductors with band gaps ranging from E_g= 0.34 eV for GaTlS (1) to E_g= 1.84 eV for TlS (1). Moreover, all compounds exhibit their highest absorption peaks in the ultraviolet (UV) range, making them efficient absorbers of sunlight for potential use in photovoltaic and photocatalytic applications. Notably, these systems demonstrate low rates of charge carrier recombination due to the presence of a built-in electric field (in Janus structures) or their indirect band gap character. Additionally, except for ATlS (1), the compounds show promise as photocathodes for hydrogen production even through seawater splitting, pH= 8.3, with an absolute value of the Gibbs free energy change$|\Delta G| < 1.5$ eV. In contrast, InTlS (1) emerges as an exceptionally promising material for applications in highly acidic environments, exhibiting a ΔG of about$- 0.53$ eV.

---
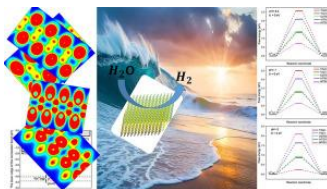
88. Water wave scattering by a thick rectangular rigid barrier over a non-uniform monotonically

decreasing oscillatory bathymetry
D Goyal, SC Martha - Ocean Engineering, 2024

Abstract: The current study uses a linearized two-dimensional model to examine the impact of scattering of waves by a thick rigid barrier over the non-uniform coastal bed morphology in three different configurations; namely, the barrier lies above the bottom profile (Type I), barrier lies on the left of the bottom profile (Type II), and the barrier lies on the right of the bottom profile (Type III). The non-uniform bathymetry is characterized by a monotonically decreasing oscillatory profile in which the decay factor controls the non-uniformity and can effectively capture the impact of uneven characteristics of the morphology of the coastal bed. To determine the transmission and reflection coefficients, we employed a computationally efficient boundary element method in conjunction with the eigenfunction expansion strategy. An energy balance relation based on energy flux conservation is obtained and is further satisfied by the numerical values of reflection and transmission coefficients. The study reveals that the Bragg resonance peak amplifies by raising the decay factor and submergence depth in all three types of configurations, which improves the undulating profile and barrier's wave-reflecting capabilities, ultimately benefiting the coastal areas. A qualitative phase shift behavior of the Bragg resonance peak is also found. It predicts that phase shift occurs in a non-monotonic manner with the rise in the width of the barrier in Type I configuration, while it occurs in a monotonic manner with an increase in width in Type II and Type III configurations. A threshold value for barrier thickness equal to 3 is obtained in the current analysis to obtain nearly 80% reflection, and further increase in thickness has no discernible effect beyond this threshold. The study also found that changes in the height of bottom undulation have a significant effect on low-frequency waves but a very minimal effect on high-frequency waves. These observations can help ocean engineers to design an effective breakwater that is economically efficient and simpler in geometry to safeguard coastal regions with non-uniform morphology.